The Wavenumber–Frequency Content of Resonantly Excited Equatorial Waves

THEODORE S. DURLAND

College of Oceanic and Atmospheric Sciences, Oregon State University, Corvallis, Oregon

J. THOMAS FARRAR

Woods Hole Oceanographic Institution, Woods Hole, Massachusetts

(Manuscript received 12 December 2011, in final form 9 May 2012)

ABSTRACT

The theoretical resonant excitation of equatorial inertia–gravity waves and mixed Rossby–gravity waves is examined. Contrary to occasionally published expectations, solutions show that winds that are broadband in both zonal wavenumber and frequency do not in general produce peaks in the wavenumber–frequency spectrum of sea surface height (SSH) at wavenumbers associated with vanishing zonal group velocity.

Excitation of total wave energy in inertia–gravity modes by broadband zonal winds is virtually wavenumber independent when the meridional structure of the winds does not impose a bias toward negative or positive zonal wavenumbers. With increasing wavenumber magnitude $|k|$, inertia–gravity waves asymptote toward zonally propagating pure gravity waves, in which the magnitude of meridional velocity v becomes progressively smaller relative to the magnitude of zonal velocity u and pressure p. When the total wave energy is independent of wavenumber, this effect produces a peak in $|v|^2$ near the wavenumber where group velocity vanishes, but a trough in $|p|^2$ (or SSH variance). Another consequence of the shift toward pure gravity wave structure is that broadband meridional winds excite inertia–gravity modes progressively less efficiently as $|k|$ increases and v becomes less important to the wave structure. Broadband meridional winds produce a low-wavenumber peak in total wave energy leading to a subtle elevation of $|p|^2$ at low wavenumbers, but this is due entirely to the decrease in the forcing efficiency of meridional winds with increasing $|k|$, rather than to the vanishing of the group velocity. Physical conditions that might alter the above conclusions are discussed.

1. Introduction

Wunsch and Gill (1976, hereafter WG) stimulated the field of equatorial oceanography with a demonstration that spectral peaks at periods of 3–5 days in Pacific Ocean tide gauge records could be interpreted as being due to equatorially trapped inertia–gravity waves. In what was one of the earliest observational validations of linear equatorial wave theory applied to the oceans, they showed that the latitudinal dependence of spectral power in these peaks agreed reasonably well with the theoretically predicted structures of the appropriate meridional modes. They also showed that the peaks fell near the minimum frequencies of the theoretical modes—that is, the frequencies associated with vanishing zonal group velocity.

WG did not attempt wavenumber estimates, but they suggested that it was physically reasonable to find energy accumulating at the wavenumber associated with vanishing group velocity for free waves, where energy cannot escape the generating region. They also pointed out that their results were equally compatible with SSH variability being excited at near-zero zonal wavenumbers by basin-scale winds. For a given mode, the relative difference in the frequencies predicted by these two distinct hypotheses is at most 1.5% (WG). The short sea level records did not allow WG to distinguish between the two predictions, but their mathematical analysis suggested that the latter of these hypotheses was the more likely. Nevertheless, the association of oceanic resonances with vanishing group velocity has lived on to the extent that subsequent authors have stated or implied that we might expect to find excess energy at the wavenumber of

Corresponding author address: Ted Durland, College of Oceanic and Atmospheric Sciences, Oregon State University, Corvallis, OR 97331.
E-mail: tdurland@coas.oregonstate.edu

DOI: 10.1175/JPO-D-11-0234.1

vanishing zonal group velocity and have cited WG as the source of the expectation (e.g., LeBlond and Mysak 1978; Luther 1980; Garzoli and Katz 1981; Lin et al. 2008; Ferrari and Wunsch 2010).

The idea of excess energy accumulating at the wavenumber of vanishing group velocity is physically reasonable, and in the summary we discuss some of the conditions proposed by Luther (1980) under which this might occur. The tenacity of the idea that such a physical process was demonstrated theoretically by WG is somewhat curious, however, because it is not in fact what the mathematics of WG predicted. In the analysis that led them to expect excess energy in frequency spectra near modal frequency minima, the resonant energy produced by a broadband forcing spectrum was the same order of magnitude everywhere along a free-wave dispersion curve. It was only after the theoretical transfer function was integrated over all wavenumbers to produce a frequency spectrum that elevated energy was found near the frequency minimum. The reason is simply that when a dispersion curve has a local frequency extremum, the wavenumber band containing points ''near'' the dispersion curve is broader near that extremum than at other frequencies. This point had been brought out previously by Longuet-Higgins (1965) and Blandford (1966). Forcing that is broadband in wavenumber and frequency can be expected to produce a peak in a frequency spectrum at the frequency where a dispersion curve parallels the wavenumber axis, but nowhere in any of the above analyses can be found a prediction of elevated energy in wavenumber–frequency space at the locus of vanishing group velocity.

In spite of their prediction of a peak in the frequency spectrum at a modal frequency minimum, WG found that in the presence of broadband forcing the peak drops off slowly with increasing frequency, causing it to be skewed toward higher frequencies in a manner that did not resemble the observations. This led to the prescient observation that the oceanic peaks must be forced by winds concentrated in a relatively narrow low-wavenumber band: their other hypothesis. This prediction has been borne out (e.g., Luther 1980; Farrar and Durland 2012), and it appears that the locations of the spectral peaks in equatorial sea level may owe more to the concentration of equatorial wind energy in low wavenumbers than to special characteristics of the vanishing-group-velocity locus (see Farrar and Durland 2012).

Because the classic paper by WG is often misinterpreted, we feel that it is important to revisit their analysis for the sake of clarification. In addition, we find that resonant solutions for meridional velocity (the mathematically convenient proxy for equatorial wave amplitude) reveal considerable wavenumber dependence that is not captured by the order-of-magnitude solutions of WG, and that the wavenumber dependence of wave pressure (the appropriate proxy for SSH) is significantly different from that of meridional velocity. Accordingly, we examine in greater detail the wavenumber–frequency dependence of resonant equatorial inertia–gravity and mixed Rossby–gravity (MRG) waves in the presence of broadband wind forcing. The goal is to understand the wavenumber–frequency dependence of the equatorial ocean's tendency toward resonance, independent of the wavenumber–frequency structure imposed by the wind. Several idealized meridional structures for the wind forcing are considered, but the forcing is considered to be independent of wavenumber and frequency in all scenarios.

We will use the theory of linear waves on a quiescent background throughout the paper, as did WG. The theoretical work of McPhaden and Knox (1979) and the observations of Farrar and Durland (2012) indicate that the currents of the equatorial Pacific have only minor effects on the rest-state solutions for the high frequency waves considered here. Section 2 reviews the linear theory (following WG and Moore and Philander 1977, hereafter MP), introducing notation and emphasizing points that will facilitate later interpretations.

2. Equations and free-wave solutions

The nondimensional equations for a single baroclinic mode on the equatorial β plane, Fourier transformed in time t and the zonal dimension x, are as follows:

$$-i\omega u - yv + ikp = -\epsilon u + X, \tag{1}$$

$$-i\omega v + yu + p_y = -\epsilon v + Y, \quad \text{and} \tag{2}$$

$$-i\omega p + iku + v_y = -\epsilon p. \tag{3}$$

Length and time have been nondimensionalized by the equatorial length and time scales, $L_e = \sqrt{c/\beta_0}$ and $T_e = 1/\sqrt{\beta_0 c}$, where c is the high-frequency gravity wave speed of the baroclinic mode and β_0 is the meridional gradient of the Coriolis parameter at the equator. Pressure (p) is nondimensionalized by $\rho_0 c^2$, where ρ_0 is the mean water density. In the central equatorial Pacific, typical values of L_e and T_e are 350 km and 1.4 days for the first baroclinic mode, and 273 km and 1.9 days for the second baroclinic mode. The x and t dependence is $e^{i(kx-\omega t)}$, and y represents both the northward coordinate and the Coriolis parameter. Eastward and northward components of the current are u and v.

The momentum forcing terms, X and Y, are the projections of the vertical distributions of shear stress onto

the baroclinic modal structure, and they are proportional to the zonal and meridional wind stress, respectively. We are only interested in relative amplitudes and will generally consider X and Y to be $O(1)$.

As pointed out by WG, the zonal wavenumbers of the solutions we consider are much smaller than the meridional wavenumbers, and the mean meridional wavenumber of a single meridional mode changes little over the parameter space we consider. For a single merdional and baroclinic mode, any scale-dependent parameterization of horizontal and/or vertical momentum diffusion can thus be reasonably represented by a constant Rayleigh dissipation parameter ϵ, which has been nondimensionalized by T_e^{-1}. We seek qualitative insight and will not be concerned with the specific value of ϵ, but require only that $\epsilon \ll \omega$ so that resonances are possible. Based on the structures of the observed frequency peaks, WG estimated that $0.05 < \epsilon < 0.1$. For our figures, we use the lower of these values. The biggest deficiency of (1)–(3) (also pointed out by Wunsch and Gill) is that the Prandtl number is set to unity, which is physically unrealistic for the oceans. As long as ϵ remains small, however, this does not detract materially from the qualitative value of the solutions.

Reducing (1)–(3) to a single differential equation in v, we have the following:

$$\sigma[v_{yy} - y^2 v + (\sigma^2 - k^2 - k/\sigma)v] = \sigma y X + k X_y + i(\sigma^2 - k^2)Y, \quad (4)$$

$$u = i(\sigma^2 - k^2)^{-1}(\sigma y v - k v_y + \sigma X), \quad \text{and} \quad (5)$$

$$p = i(\sigma^2 - k^2)^{-1}(k y v - \sigma v_y + k X), \quad \text{where} \quad (6)$$

$$\sigma \equiv \omega + i\epsilon. \quad (7)$$

a. Free waves

Without dissipation and forcing ($\epsilon = X = Y = 0$) and with boundedness conditions as $y \to \pm\infty$, the eigenvalues of (4) are the odd positive integers, yielding a dispersion relation

$$D_m \equiv \omega[\omega^2 - k^2 - k/\omega - (2m + 1)] = 0, \quad m = 0, 1, 2, \ldots, \quad (8)$$

where D_m is the "undamped dispersion polynomial." The eigenfunctions are the orthonormal Hermite functions, $\psi_m(y)$ (defined in MP).

For later use in the forced solutions, we define a "unit amplitude free wave" in terms of the amplitude of the meridional velocity. Using capital letters to denote these unit-amplitude solutions, the expressions for the wave components are

$$V_{(m)}(y) = \psi_m(y), \quad (9)$$

$$U_{(m)}(y, k) = \frac{i}{\sqrt{2}}\left[\frac{\sqrt{m+1}}{\omega_m - k}\psi_{m+1}(y) + \frac{\sqrt{m}}{\omega_m + k}\psi_{m-1}(y)\right], \quad \text{and} \quad (10)$$

$$P_{(m)}(y, k) = \frac{i}{\sqrt{2}}\left[\frac{\sqrt{m+1}}{\omega_m - k}\psi_{m+1}(y) - \frac{\sqrt{m}}{\omega_m + k}\psi_{m-1}(y)\right]. \quad (11)$$

The subscript on ω_m indicates that it satisfies the dispersion relation of mode m for the given value of k. When we wish ω to be an independent variable and k to be constrained by the dispersion relation, we will apply the modal subscript to the wavenumber: (ω, k_m). When $m = 0$, the last term on the right-hand-side (rhs) of (10) and of (11) vanishes.

The parentheses around the mode number in the subscripts of $V_{(m)}$, $U_{(m)}$, and $P_{(m)}$ indicate that these are meridional modal structures (i.e., functions of y). This notation will be used only for the wave components, and it is intended to distinguish the y-dependent modal structures from Hermite expansion coefficients that will be introduced in the next section. It is important to note that defining the relations (9)–(11) as "unit amplitude" is merely a mathematical convenience because $V_{(m)}(y)$ is the variable in which the mathematical problem was posed, and it is the only wave-field variable expressible in terms of a single Hermite function. For inertia–gravity waves, the amplitudes of $U_{(m)}$ and $P_{(m)}$ grow monotonically with increasing $|k|$, and for MRG waves they do so with increasing k; they do not remain $O(1)$ even though by definition they are still components of the "unit amplitude" free wave.

The Hermite functions are symmetric or antisymmetric about $y = 0$ depending on whether the mode number is even or odd, and the symmetry about the equator of $U_{(m)}$ and $P_{(m)}$ is opposite to that of $V_{(m)}$. We will use the symmetry of $P_{(m)}$ as a proxy for the wave symmetry, so odd numbered meridional modes are considered symmetric and even numbered modes are considered antisymmetric.

Unless otherwise noted, our analyses will be limited to the wavenumber and frequency range $|k| < 2.5$, $0.35 < \omega < 4$, which excludes the low-frequency Rossby wave solutions of (8) and allows certain simplifications in the expressions for resonant solutions. Larger zonal wavenumbers would exceed the meridional wavenumbers of

the low meridional modes, invalidating our use of a constant dissipation parameter. In dimensional units, the above range corresponds to wavelengths greater than 8.0 degrees longitude and periods between 2.3 and 26 days for the first baroclinic mode in the central equatorial Pacific. For the second baroclinic mode, these limits are 6.2 degrees and 2.9–33 days. The wavenumber–frequency range thus defined exceeds the one examined by Farrar and Durland (2012) in a companion study using daily-averaged data from the Tropical Atmosphere Ocean (TAO)/Triangle Trans-Ocean Buoy Network (TRITON) mooring array in the Pacific.

b. Comments on the free-wave dispersion relations

The dispersion diagrams for the MRG wave ($m = 0$) and the lowest four meridional modes of inertia–gravity waves ($m = 1$ through 4) are shown in the top panel of Fig. 1. As the frequency increases, the dispersion curves of all the inertia–gravity modes approach the asymptotes $\omega = \pm k$: the high-frequency gravity wave dispersion relations. These dispersion curves are similar to those of Poincaré modes in a channel (e.g., Pedlosky 2003, Fig. 13.9), except that they are skewed by the beta effect. The cutoff, or minimum frequency for a given mode ω_{cm}, and its associated wavenumber k_{cm} locate the point in wavenumber–frequency space where the group velocity of mode m vanishes. The beta effect reduces ω_{cm} slightly and shifts k_{cm} off the $k = 0$ axis toward negative wavenumbers, as can be seen from the dimensional relation: $k^*_{cm} = -\beta/2\omega^*_{cm}$. The skewing of the dispersion curve is most pronounced for the gravest meridional mode (with lowest ω_{cm}).

The MRG wave has strictly eastward group velocity. Its dispersion relation

$$k_0 = \omega - 1/\omega \tag{12}$$

asymptotes to $\omega = k$ as $k \to \infty$. The asymptote $\omega = k$ is the dispersion relation of the equatorial Kelvin wave (labeled, following Matsuno 1966, as $m = -1$), with structure

$$V_{(-1)} \equiv 0, \quad \text{and} \tag{13}$$

$$U_{(-1)} = P_{(-1)} = \psi_0(y). \tag{14}$$

The $\omega = -k$ asymptote satisfies the $m = 0$ and $m = -1$ dispersion relations for modes with westward group velocity. These modes are inadmissible on the infinite β plane because their p and u signals are unbounded. They can exist in a more realistically bounded basin, but energy associated with them would be concentrated near the poleward boundaries.

c. Comments on free-wave meridional structures

As the dispersion curve of an inertia–gravity mode approaches an asymptote, one of the denominators on the rhs of (10) and (11) approaches zero, and the associated term comes to dominate the wave component structure: as $k \to \pm\infty$, $U_{(m)} \to \pm P_{(m)}$ and the meridional structure of both approaches $\psi_{m\pm1}(y)$. Also, both

$$\begin{aligned}&(\max_y|U_{(m)}|/\max_y|V_{(m)}|) \quad \text{and}\\ &(\max_y|P_{(m)}|/\max_y|V_{(m)}|) \to \infty \quad \text{as} \quad |k| \to \infty,\end{aligned} \tag{15}$$

where $\max_y$ refers to the meridional maximum at a given k. With increasing $|k|$, the waves are asymptoting toward zonally propagating pure gravity waves in which the wave particle trajectories align with the phase propagation direction, $V_{(m)}$ is insignificant relative to $U_{(m)}$, and the particle velocity in the direction of propagation is proportional to and in phase with the pressure. The tendency toward the above limits is occurring even at small wavenumbers. It is possible, for instance, for a peak in the wavenumber–frequency spectrum of $|V_{(m)}|^2$ at the locus of vanishing group velocity to be associated with a trough in the spectrum of $|P_{(m)}|^2$ at the same location. Because the dispersion curve of a given mode is skewed toward negative wavenumbers, at any given frequency the wave with westward group velocity is closer to the gravity wave limit than the wave with eastward group velocity.

In (15) it would be more realistic to think of the wave meridional velocity decreasing as the wave approaches the gravity wave limit, rather than thinking of the $U_{(m)}$ and $P_{(m)}$ amplitudes as increasing without bound. Pegging the ''unit amplitude'' definition to the amplitude of $V_{(m)}$, however, avoids unnecessary mathematical complexities and is no problem as long as we remember that it is just a mathematically useful convention.

Figure 1 illustrates the wavenumber dependence of $U_{(m)}(y)$ and $P_{(m)}(y)$ by displaying the meridional structures of the wave components for meridional mode 1 at $k = 0$ and at the positive and negative wavenumbers associated with $\omega = 2.8$. The important point to note is that while the amplitude and meridional structure of $V_{(m)}$ remain unchanged over all k, this is not true of $U_{(m)}$ and $P_{(m)}$. The structures of $U_{(m)}$ and $P_{(m)}$, including the latitudes of their extrema and zero crossings, are functions of wavenumber. The only meaningful definition of ''amplitude'' for one of these variables that is consistent for a single mode over all wavenumbers therefore involves the integrated variance, from which the amplitude

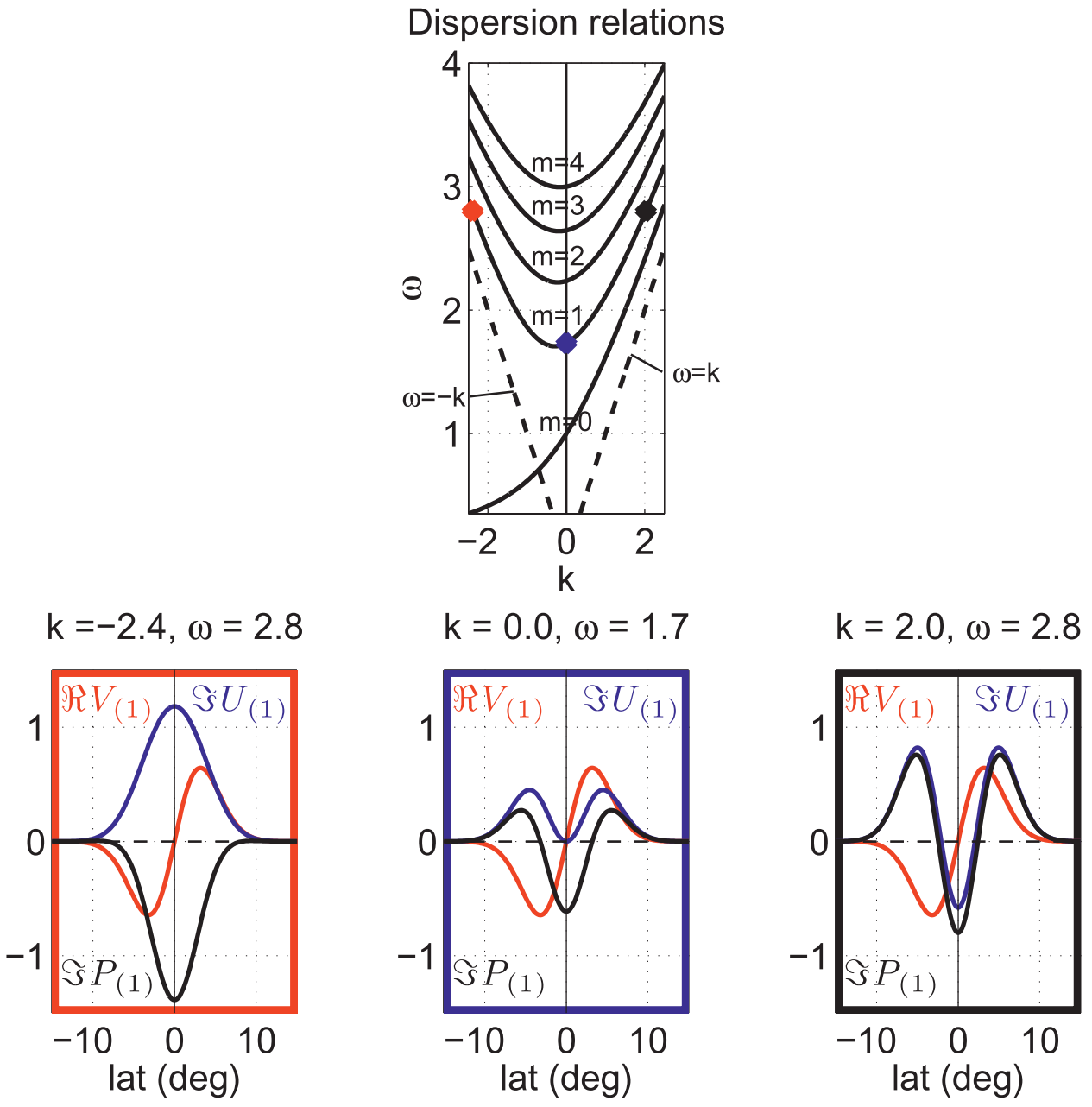

FIG. 1. (top) Dispersion curves for unforced MRG wave ($m = 0$) and lowest four meridional modes of inertia–gravity waves. (bottom) Meridional structures of meridional mode-1, unit amplitude free-wave components. The color of the box in a bottom panel corresponds to the color of the dot on the $m = 1$ dispersion curve in the top panel where the wave structures were calculated. In each bottom panel, the real part of the meridional velocity is displayed in red, while the imaginary parts of the zonal velocity and pressure are displayed in blue and black, respectively. Note that the structure and amplitude of the meridional velocity do not change with wavenumber. Both the structure and the amplitude of zonal velocity and pressure are wavenumber dependent. Latitude has been scaled appropriately for baroclinic mode 1 in the central equatorial Pacific. Equivalent structures for baroclinic mode 2 are compressed toward the equator by about 20%.

at any latitude can be deduced for a given wavenumber. We define

$$\langle |P_{(m)}|^2 \rangle \equiv \int_{-\infty}^{\infty} |P_{(m)}|^2 \, dy, \tag{16}$$

and the orthonormality of the Hermite functions gives

$$\langle |V_{(m)}|^2 \rangle = 1, \quad \text{and} \tag{17}$$

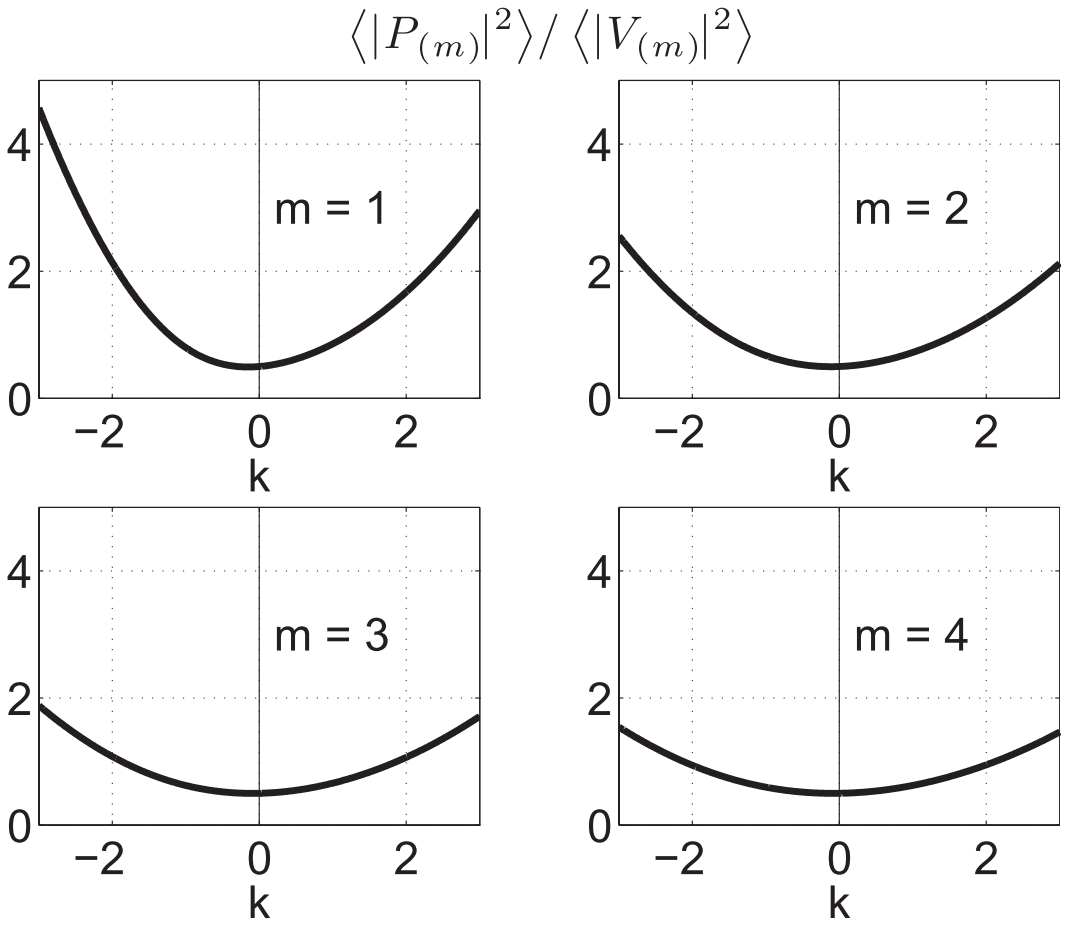

FIG. 2. Wavenumber dependence of the ratio of integrated pressure variance to integrated meridional velocity variance for the free inertia–gravity waves, where the integration is over latitude; meridional modes 1–4. This ratio is exactly the integrated variance of pressure for the ''unit amplitude'' wave because the integrated variance of meridional velocity is 1 by definition for this wave. We retain the ratio designation to emphasize its use as a conversion factor between forced solutions for meridional velocity and those for pressure. The minimum falls between $k = 0$ and the wavenumber associated with vanishing group velocity.

$$\langle |P_{(m)}|^2 \rangle = \langle |U_{(m)}|^2 \rangle = \frac{1}{2}\left[\frac{m+1}{(\omega_m - k)^2} + \frac{m}{(\omega_m + k)^2}\right]. \tag{18}$$

In Fig. 2 we plot $\langle |P_{(m)}|^2 \rangle / \langle |V_{(m)}|^2 \rangle$ as a function of wavenumber for the lowest four meridional modes. Because of (17), this is just $\langle |P_{(m)}|^2 \rangle$ for the unit amplitude wave. We will retain the ratio notation as a reminder, however, because this term will be used to convert forced-wave solutions for meridional velocity to solutions for pressure. As expected from (15), $\langle |P_{(m)}|^2 \rangle / \langle |V_{(m)}|^2 \rangle$ increases with increasing $|k|$, it increases faster on the $k < 0$ branch, and the associated asymmetry (due to the beta effect) decreases with increasing mode number.

The MRG wave structure is

$$V_{(0)}(y) = \psi_0(y), \quad \text{and} \tag{19}$$

$$U_{(0)}(y) = P_{(0)}(y) = \frac{i}{\sqrt{2}}\omega\psi_1(y). \tag{20}$$

The meridional structures of $U_{(0)}$ and $P_{(0)}$ do not change with wavenumber, but the ratios $(\max_y|U_{(0)}|/\max_y|V_{(0)}|)$ and $(\max_y|P_{(0)}|/\max_y|V_{(0)}|)$ increase monotonically with increasing frequency, and hence with increasing wavenumber (rather than increasing $|k|$).

3. Forced and damped solutions

The y-dependent variables in the forced Eq. (4) are expanded in Hermite series:

$$(v, X, Y) = \sum_{m=0}^{\infty} (v_m, X_m, Y_m)\psi_m(y). \tag{21}$$

Note that we are projecting the atmospheric structures onto Hermite functions scaled to the oceanic deformation radius. A given wind structure will thus have different expansion coefficients for different oceanic baroclinic modes.

The forced wave structures are represented by lower case letters; for example,

$$v_{(m)}(y,k,\omega) = v_m(k,\omega)\psi_m(y). \tag{22}$$

As with the unit-amplitude free waves [(9)–(11)], the parentheses about the subscript indicate a function of y, while the subscript without the parentheses on v_m indicates a Hermite expansion coefficient.

With the application of (A1)–(A3) and a notation similar to that of WG, (4) reduces to

$$v_m = G_m/W_m, \tag{23}$$

where G_m is associated with the forcing terms on the rhs of (4) and W_m with the dispersion related terms on the left-hand-side (lhs) of (4). There is an arbitrariness to the definitions of G_m and W_m: a common factor can be applied to both without changing the solution. We will show later that a physically revealing way to define them is

$$G_m \equiv \frac{1}{\sqrt{2}}\left(\frac{\sqrt{m+1}}{\sigma - k}X_{m+1} + \frac{\sqrt{m}}{\sigma + k}X_{m-1}\right) + iY_m, \tag{24}$$

$$W_m \equiv [\sigma^3 - \sigma(k^2 + 2m + 1) - k]/(\sigma^2 - k^2), \tag{25}$$

and we will call G_m the ''forcing function'' and W_m the ''dispersion function.'' The full transfer function from atmospheric to oceanic Hermite components involves the ratio of G_m and W_m, but it is illuminating to examine the terms separately (as WG did).

The solution process of WG is most easily demonstrated with the alternative definitions used by WG, which we will identify with script notation:

$$\mathcal{G}_m \equiv (\sigma^2 - k^2)G_m, \quad \text{and} \tag{26}$$

$$\mathcal{W}_m \equiv (\sigma^2 - k^2)W_m. \tag{27}$$

The latter of these terms was called the ''dispersion polynomial'' by WG, and it is identical in form to our undamped dispersion polynomial D_m in (8), with the oscillation frequency ω replaced by the complex frequency σ.

We will be concerned with power spectra:

$$|v_m|^2 = |G_m|^2/|W_m|^2 = |\mathcal{G}_m|^2/|\mathcal{W}_m|^2, \tag{28}$$

and we note that the squared magnitude of the dispersion polynomial can be written

$$|\mathcal{W}_m|^2 = D_m^2 + \epsilon^2[3\omega^4 + 6\omega k + (k^2 + 2m + 1)^2] + O(\epsilon^4). \tag{29}$$

For $\epsilon \ll \omega$, $|\mathcal{W}_m|^2$ is approximately minimized and $|v_m|^2$ is approximately maximized (achieving resonance) on the undamped free-wave dispersion curve for mode m, where $D_m = 0$. We are looking for solutions where $\omega = O(1)$, so our condition that $\epsilon \ll \omega$ implies that $\epsilon \ll 1$.

a. Order of magnitude solutions of Wunsch and Gill

WG assumed randomized forcing, so that the frequency spectrum at an arbitrary point in space is simply an integral over all wavenumbers of the wavenumber–frequency spectrum. For a representation of broadband forcing, WG assumed that $\mathcal{G}_m$ was independent of wavenumber and frequency, giving the following expression for the frequency spectrum:

$$S(\omega) \equiv \int_{k=-\infty}^{\infty} |v_m(k,\omega)|^2\, dk = |\mathcal{G}_m|^2 \int_{k=-\infty}^{\infty} \frac{1}{|\mathcal{W}_m|^2}\, dk. \tag{30}$$

At a given frequency, using the form (29) for $|\mathcal{W}_m|^2$ and expanding D_m^2 in powers of wavenumber about a point (ω, k_m) on the dispersion curve allows (30) to be expressed as

$$S(\omega) = |\mathcal{G}_m|^2 \int_{k=-\infty}^{\infty} \frac{1}{\sum_{n=2}^{4} d_n(k - k_m)^n + \delta^2}\, dk, \tag{31}$$

where δ is $O(\epsilon)$. The expansion coefficients are

$$[d_2, d_3, d_4] = [(2\omega k_m + 1)^2, 2\omega(2\omega k_m + 1), \omega^2]. \tag{32}$$

Only the wavenumber range where $\sum_{n=2}^{4} d_n(k - k_m)^n \leq O(\epsilon^2)$ contributes substantially to the integral, so only the lowest power of $(k - k_m)$ needs to be considered. The integral can thus be evaluated using the method of residues. Near a general point on a dispersion curve where $\omega > \omega_{cm}$, $d_2(k - k_m)^2 + \delta^2$ factors into two simple poles, each of $O(\epsilon)$. One of the poles is captured by the integration contour, producing an integral that is $O(\epsilon^{-1})$. At the locus of vanishing group velocity, however, $(2\omega_{cm}k_{cm} + 1) = 0$. The coefficients d_2 and d_3 vanish, leaving a denominator of $d_4(k - k_m)^4 + \delta^2$. This factors into four simple poles, with the zero in each case being $O(\epsilon^{1/2})$. The residue at each pole is therefore $O(\epsilon^{-3/2})$, so

$$S(\omega_{cm}) = S(\omega > \omega_{cm}) \times O(\epsilon^{-1/2}). \tag{33}$$

The frequency spectrum of meridional velocity at the modal frequency minimum is larger than at higher frequencies by a factor that is $O(\epsilon^{-1/2})$.

This is the essence of WG's analysis predicting elevated spectral energy at ω_{cm}. Note in (30)–(31) that $|W_m|^2 = \delta^2 = O(\epsilon^2)$ *everywhere* along a dispersion curve. The vanishing of d_2 and d_3 is due to the vanishing of $\partial D_m/\partial k$ at (ω_{cm}, k_{cm}), that is, the fact that we are at a modal frequency extremum. Having only the $(k - k_{cm})^4$ term in the denominator means that the integrand remains significant over a larger range of k than when the denominator contains the $(k - k_{cm})^2$ term. The integral at ω_{cm} is larger than at higher frequencies only because the wavenumber band contributing to the integral is largest when the dispersion curve is parallel to the k axis, as illustrated in Fig. 3. This of course occurs at a frequency extremum where the group velocity vanishes, but it is not the result of a special enhancement of the response at the locus of vanishing group velocity in wavenumber–frequency space. Both Longuet-Higgins (1965) and Blandford (1966) made this point in their own ways. Neither demonstrated an enhancement in response at the wavenumber–frequency locus of vanishing group velocity.

WG found that for reasonable values of ϵ, the $\epsilon^{-1/2}$ enhancement of the frequency spectrum near ω_{cm} fell off slowly with increasing frequency in the presence of broadband forcing. The frequency peaks were thus skewed toward higher frequencies, unlike the observed peaks (see WG, Fig. 13). WG hence concluded that the winds exciting the observed peaks must be concentrated in a relatively narrow, low-wavenumber band, a conclusion supported by Farrar and Durland (2012). This conclusion did not depend on an enhancement of spectral energy at the locus of vanishing group velocity in wavenumber–frequency space.

b. More detailed solutions

The analysis of WG was only approximate to the order of the dissipation parameter. Equations (24)–(29) show that there is a wavenumber and frequency dependence to $|v_m|^2$ at resonance that is not captured by the order-of-magnitude solution, and it is worth examining this structure in more detail. For each meridional mode, the important information is the wavenumber dependence of the response at peak resonance, which occurs on the free-wave dispersion curve. Restricting the calculations to points on a dispersion curve simplifies the mathematics and facilitates the extraction of physical insight from the equations, the focus of the next few subsections.

To better understand the final solution, we will first consider the major components of the solution separately: the forcing function $\hat{G}_m$, the dispersion function

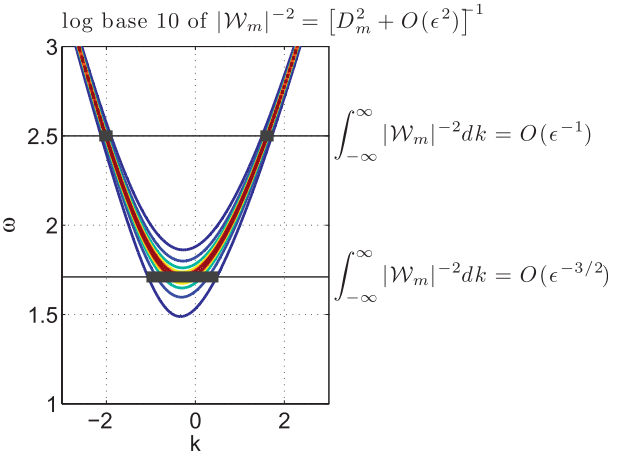

FIG. 3. Conceptual conversion from wavenumber–frequency spectrum to frequency spectrum. The integral over all wavenumbers of the inverse-square dispersion polynomial is larger at the modal frequency minimum than at higher frequencies because the band of wavenumbers that make significant contributions to the integral is largest at this frequency. Maximum resonance is found on the free-wave dispersion curve where $D_m = 0$.

$\hat{W}_m$, and the ratio of integrated pressure variance to integrated meridional-velocity variance $\langle|\hat{p}_{(m)}|^2\rangle/\langle|\hat{v}_m|^2\rangle$ (remember that $\langle|v_{(m)}|^2\rangle = |v_m|^2$). The hats on the variables indicate that they are evaluated on the meridional mode-m dispersion curve. The final solutions we will consider are the integrated meridional-velocity variance $|v_m|^2$, the integrated pressure variance $\langle|p_{(m)}|^2\rangle$ and the period-averaged, meridionally integrated total-wave energy E_m (see MP):

$$E_m \equiv (\langle|v_{(m)}|^2\rangle + \langle|u_{(m)}|^2\rangle + \langle|p_{(m)}|^2\rangle)/4. \qquad (34)$$

The variance in meridional velocity was the proxy for equatorial wave energy used by WG. It is the most convenient proxy because the mathematical problem is formulated in terms of v_m. The proper proxy for SSH variance, however, is the pressure variance, and the free wave solutions lead us to expect that its wavenumber dependence may be quite different than that of $|v_m|^2$ (e.g., Figure 2). Finally, the spectrum of the total wave energy illustrates the wavenumber–frequency dependence of the efficiency with which energy can be transmitted from the atmosphere to a particular oceanic mode.

X and Y are independent of wavenumber and frequency (''broadband''), and their phases at any particular (k, ω) are independent of latitude. Note that this is not identical to WG's approach of keeping $\mathcal{G}_m$ wavenumber- and frequency-independent [see (24) and (26)]. The choice of a meridional structure for the wind that will not predetermine the wavenumber-dependence of the response is less obvious, and we will consider a few

separate scenarios of meridional structure that provide enough insight to draw some general conclusions. These are shown in Fig. 4 and explained later.

The panels in the top rows of Figs. 5–8 show the wavenumber–frequency spectra of $\langle|v_{(m)}|^2\rangle$, $\langle|p_{(m)}|^2\rangle$ and E_m for the lowest four meridional modes of inertia–gravity waves under the various forcing scenarios. These panels are primarily illustrative, and the wavenumber dependence for each of these variables at peak resonance is plotted in the bottom row of each figure. The squared forcing function $|\hat{G}_m|^2$, the inverse squared dispersion function $|\hat{W}_m|^{-2}$, and the conversion from meridional velocity variance to pressure variance $\langle|\hat{p}_{(m)}|^2\rangle/\langle|\hat{v}_{(m)}|^2\rangle$ are shown in the middle row. The latter two terms depend only on mode number and not on the forcing, but we show them in all the figures to simplify the visual interpretation of how the various terms contribute to the final spectra. Figures 9 and 10 have the same format as Figs. 5–8, but are for the MRG waves.

For reference to an observable range of wavenumbers, the dashed vertical lines in each panel of the bottom two rows in Figs. 5–8 mark the nominal Nyquist wavenumbers of the TAO/TRITON array (±1 cycle per 30° longitude), nondimensionalized for baroclinic modes 1 and 2. Baroclinic mode 2 is represented by the lines closer to $k = 0$.

1) Forcing function at resonance

On the inertia–gravity wave dispersion curves,

$$\omega_m^2 - k^2 = 2m + 1 + k/\omega_m \rightarrow \begin{cases} 2m & \text{as} \quad k \rightarrow -\infty \\ 2(m+1/2) & \text{as} \quad k \rightarrow 0 \\ 2(m+1) & \text{as} \quad k \rightarrow \infty \end{cases}. \tag{35}$$

Likewise,

$$\omega_m + k \rightarrow m/\omega_m \quad \text{as} \quad k \rightarrow -\infty, \quad \text{and} \tag{36}$$

$$\omega_m - k \rightarrow (m+1)/\omega_m \quad \text{as} \quad k \rightarrow \infty. \tag{37}$$

On the dispersion curves, it is thus always true that

$$\sigma^2 - k^2 = (\omega_m^2 - k^2)[1 + O(\epsilon)]. \tag{38}$$

As long as $\epsilon \ll m/\omega_m$, we can also write

$$\sigma \pm k = (\omega_m \pm k)[1 + O(\epsilon)]. \tag{39}$$

Having limited ourselves to $\omega < 3.5$ and using $\epsilon = 0.05$ for our sample calculations, the above condition holds well for most of the domain.

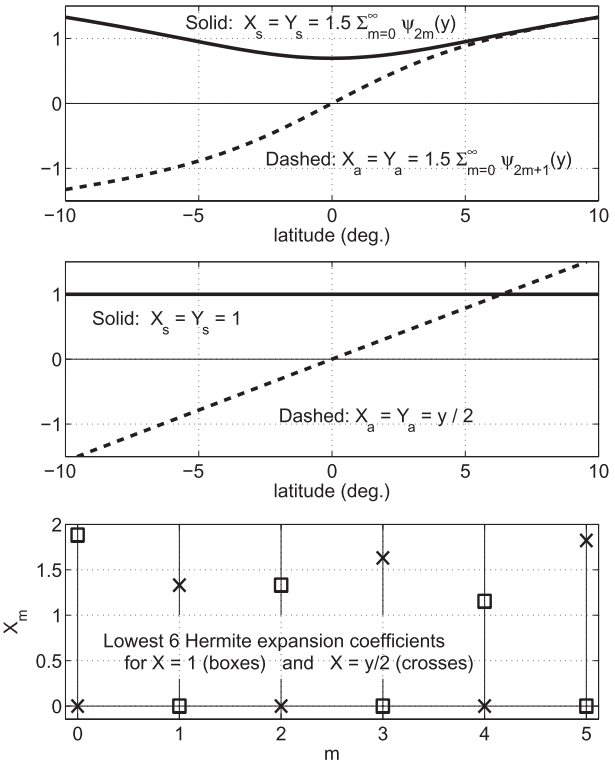

FIG. 4. Meridional structures of idealized symmetric and antisymmetric forcing scenarios: (top) structures with constant Hermite expansion coefficients, $X_s = Y_s = 1.5\sum_{n=0}^{\infty}\psi_{2n}(y)$ (solid curve), and $X_a = Y_a = 1.5\sum_{n=0}^{\infty}\psi_{2n+1}(y)$ (dashed curve); (middle) lowest-order approximations to large-scale symmetric and antisymmetric forcing structures, $X_s = 1$ (solid curve) and $X_a = y/2$ (dashed curve). In each panel, latitude is scaled appropriately for baroclinic mode 1. (bottom) Lowest six Hermite expansion coefficients for $X_s = 1$ (boxes) and $X_a = y/2$ (crosses).

Over the wavenumber–frequency range we are considering then, the forcing function at resonance can be written as

$$\hat{G}_m = \frac{1}{\sqrt{2}}\left(\frac{\sqrt{m+1}}{\omega_m - k}X_{m+1} + \frac{\sqrt{m}}{\omega_m + k}X_{m-1}\right) + iY_m + O(\epsilon). \tag{40}$$

Comparing (40) with (9) and (10), we see that on the dispersion curve, the forcing function is simply the projection of the zonal forcing's meridional structure onto that of the unit-amplitude free-wave's zonal velocity, combined with the projection of the meridional forcing's meridional structure onto that of the unit-amplitude free-wave's meridional velocity:

$$\hat{G}_m = i[\langle V_{(m)}Y\rangle - \langle U_{(m)}X\rangle] + O(\epsilon). \tag{41}$$

The negative sign in (41) is merely a reflection of the 90° phase difference between $U_{(m)}$ and $V_{(m)}$ combined with

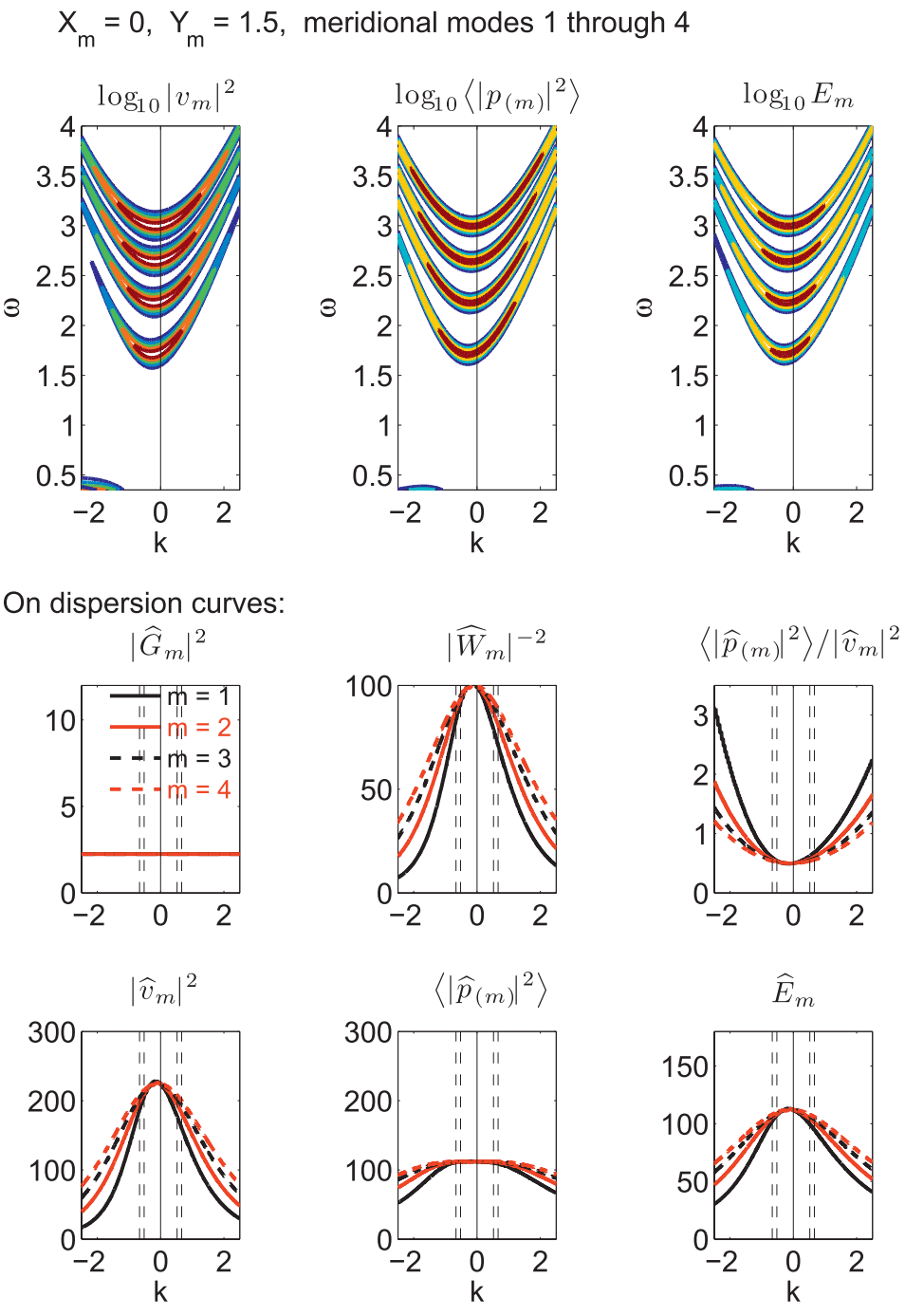

FIG. 5. Response of lowest 4 oceanic meridional modes to meridional winds with meridional structures characterized by constant Hermite expansion coefficients (top panel, Fig. 4). Symmetric oceanic meridional modes (m odd) are forced by the antisymmetric $Y_a = 1.5\sum_{n=0}^{\infty}\psi_{2n+1}(y)$. Antisymmetric oceanic modes (m even) are forced by the symmetric $Y_s = 1.5\sum_{n=0}^{\infty}\psi_{2n}(y)$. (top) Wavenumber–frequency spectra of log base 10 of (left to right) meridional velocity $|v_m|^2$, integrated pressure $\langle|p_{(m)}|^2\rangle$ and total wave energy E_m. (middle) Wavenumber dependence of contributions to resonance solutions, calculated on the free-wave dispersion curves (at maximum resonance). (left to right) the squared forcing function $|\hat{G}_m|^2$ [see (40)–(41)], the inverse squared dispersion function $|\hat{W}_m|^{-2}$ [see (46)] and the ratio of integrated squared pressure to integrated squared meridional velocity $\langle|\hat{p}_{(m)}|^2\rangle/|\hat{v}_m|^2$ [see (17)–(18)]. (bottom) Wavenumber dependence of the spectra in the top row, calculated on the free-wave dispersion curves (at maximum resonance). (left to right) $|\hat{v}_m|^2$, $\langle|\hat{p}_{(m)}|^2\rangle$ and $\hat{E}_m$. Mode numbers are as labeled in the middle left panel. Dashed vertical lines show the nominal Nyquist wavenumbers of the TAO/TRITON array (±1 cycle per 30° longitude) for baroclinic modes 1 and 2 (nearest $k = 0$).

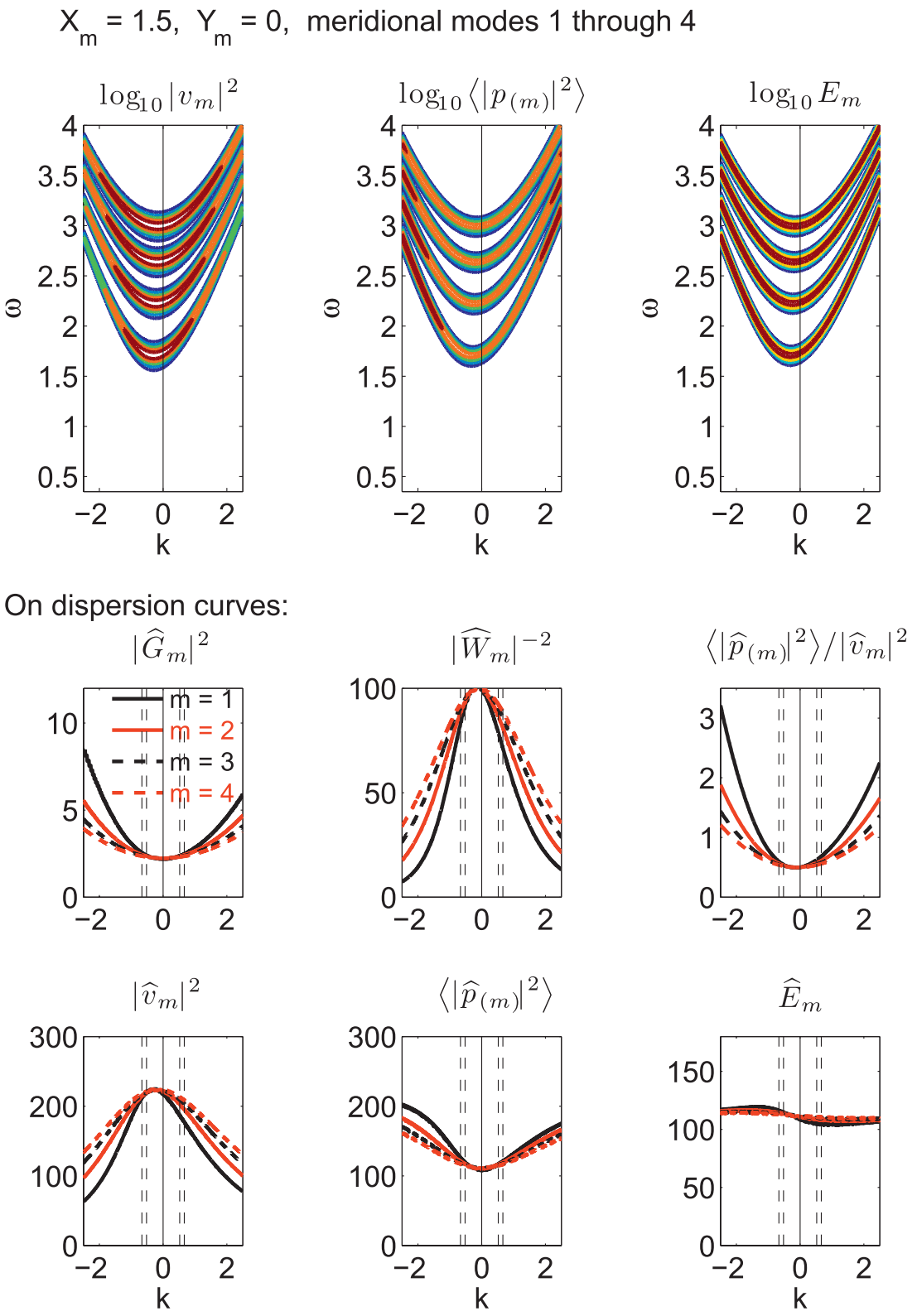

FIG. 6. Response of lowest four oceanic meridional modes to zonal winds with meridional structures characterized by constant Hermite expansion coefficients (top panel, Fig. 4). Symmetric oceanic meridional modes (m odd) are forced by the symmetric $X_s = 1.5\sum_{n=0}^{\infty}\psi_{2n}(y)$. Antisymmetric oceanic modes (m even) are forced by the antisymmetric $X_a = 1.5\sum_{n=0}^{\infty}\psi_{2n+1}(y)$. Figure format as in Fig. 5.

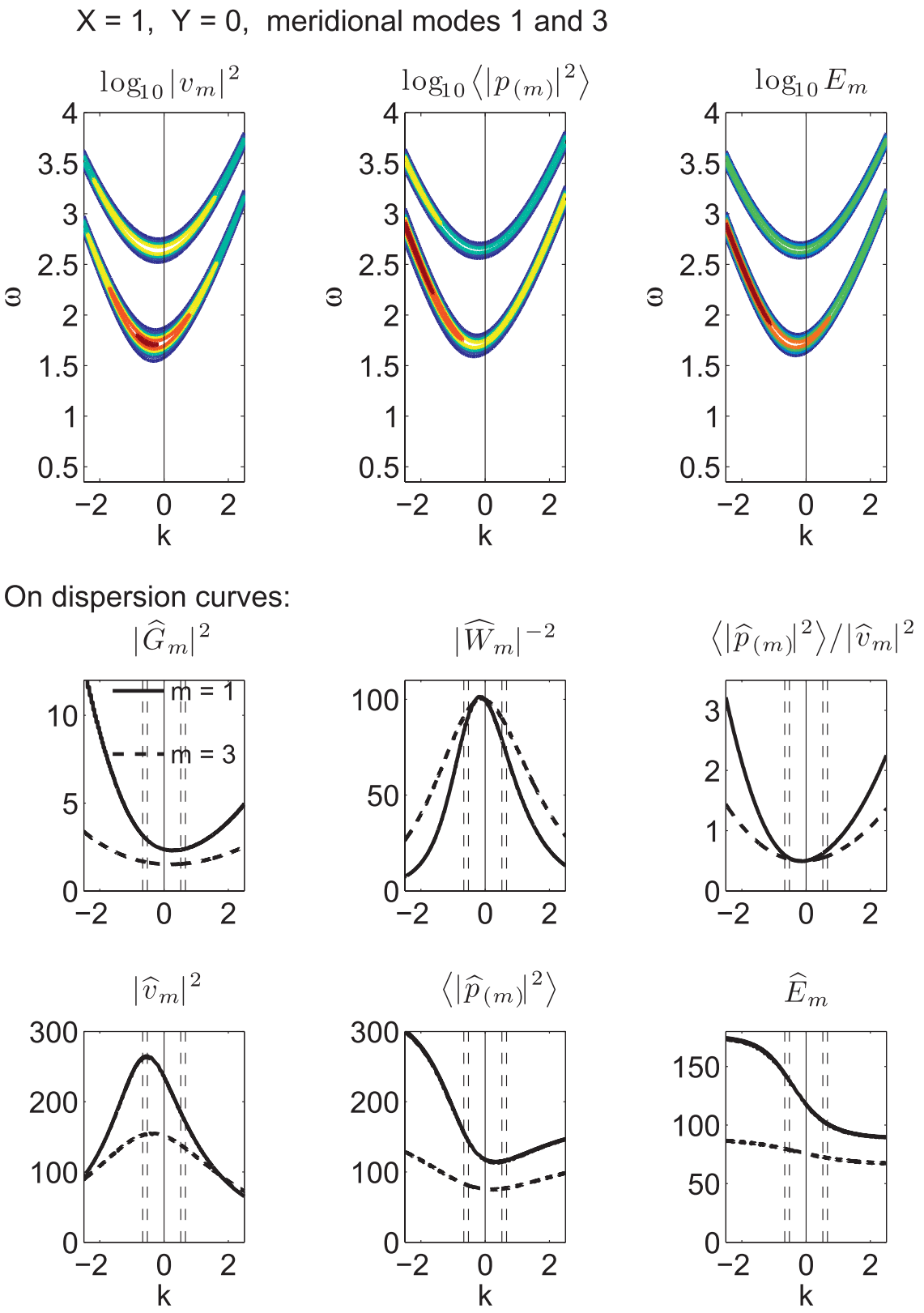

FIG. 7. Response of oceanic modes 1 and 3 to zonal winds that are uniform in latitude: $X_s = 1$ (middle panel, Fig. 4). Figure format as in Fig. 5.

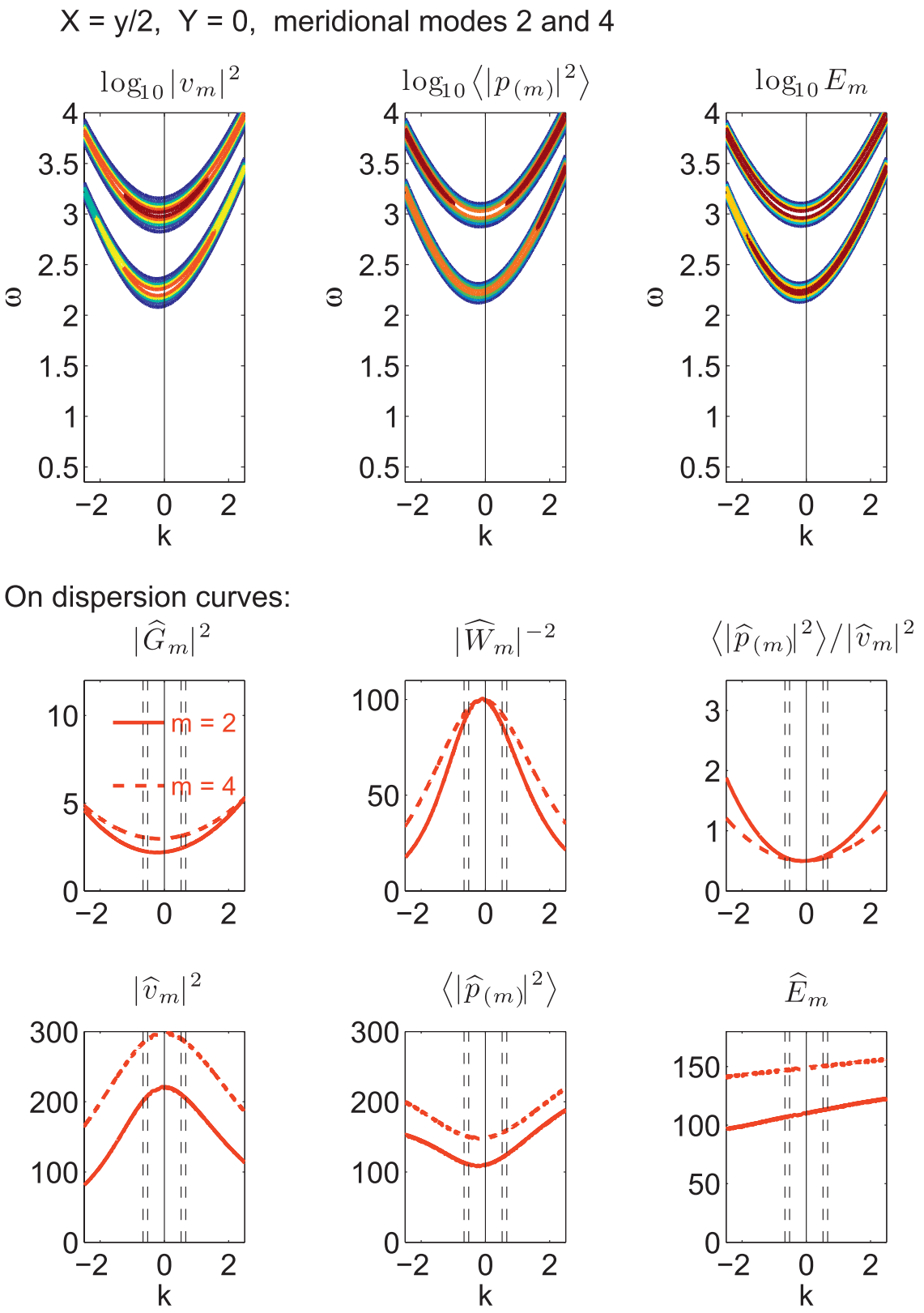

FIG. 8. Response of oceanic modes 2 and 4 to antisymmetric zonal winds: $X_a = y/2$ (middle panel, Fig. 4). Figure format as in Fig. 5.

the 90° phase difference between the way that X and Y force $v_{(m)}$.

Our choice of form for G_m makes the modal forcing term (41) analogous to the forcing of an energy equation formed directly from the nontransformed versions of (1)–(3) and integrated over the meridional domain:

$$\partial_t \frac{\langle u^2 + v^2 + p^2 \rangle}{2} = -\partial_x \langle up \rangle - 2\epsilon \frac{\langle u^2 + v^2 + p^2 \rangle}{2} + \langle uX \rangle + \langle vY \rangle . \quad (42)$$

In (42), the dependent variables are physical variables rather than their wavenumber–frequency transforms, and the projections $\langle uX \rangle$ and $\langle vY \rangle$ contain the wave amplitude as well as structure, so the correspondence between (42) and (41) is not exact. The analogy motivates our choice of form for the forcing function, however, and (41) distills the important information about the relative forcing efficiency of zonal and meridional winds, as well as the effects of various meridional structures of the winds. It also clearly represents the physical principle that energy is only added to a moving system by forcing in the direction of motion.

Taking advantage of the equatorial symmetries of the free-wave components, (41) can be decomposed into

$$\hat{G}_{2n} = i[\langle V_{(2n)} Y_s \rangle - \langle U_{(2n)} X_a \rangle] + O(\epsilon), \quad \text{and} \quad (43)$$

$$\hat{G}_{2n+1} = i[\langle V_{(2n+1)} Y_a \rangle - \langle U_{(2n+1)} X_s \rangle] + O(\epsilon), \quad n = 0, 1, 2, \ldots , \quad (44)$$

where Y_s and Y_a are the symmetric and antisymmetric parts of the meridional forcing, and similarly for the zonal forcing. An antisymmetric oceanic mode ($\hat{G}_{2n}$) is forced by symmetric meridional winds and antisymmetric zonal winds, while a symmetric oceanic mode ($\hat{G}_{2n+1}$) is forced by symmetric zonal winds and antisymmetric meridional winds.

WG postulated that the equatorial Pacific winds were dominantly symmetric about the equator, and the analysis of TAO/TRITON wind measurements by Farrar and Durland (2012) confirms this for the wavenumber–frequency band of interest. As is evident in (43) and (44), however, it is not so much the symmetry of the individual wind components that matters as the ratio of the symmetric part of one component to the antisymmetric part of the other. In the 8–17-day period band containing first and second baroclinic mode MRG waves, for instance, Farrar and Durland (2012) show that, although both zonal and meridional wind stresses are dominantly symmetric, the antisymmetric zonal wind stress can actually exceed the symmetric meridional wind stress. Estimation of the relative efficiency of the two projections in (43) requires knowledge of both the relative amplitudes of $V_{(0)}$ and $U_{(0)}$ (which can be deduced from Figs. 9–10) and the Hermite structure of the wind stress components, which was beyond the scope of Farrar and Durland's (2012) analysis. At first approximation however, it appears that both the zonal and meridional winds can contribute to the excitation of the MRG waves, in spite of the dominant symmetry of each component.

Furthermore, even relatively small amounts of energy in the antisymmetric part of the wind stress could have significant effects on the resonant energy. Let us assume, for instance, that the two projections in (44) are equally efficient, but that $|X_s|^2/|Y_a|^2 = 10$, a degree of symmetry that is exceeded in only a small portion of the wavenumber–frequency space analyzed by Farrar and Durland (2012). If X_s and Y_a are coherent, elementary algebra shows that depending on the phase relations between the two components, $|\hat{G}_{2n} + 1|^2$ could be as much as 50% lower or 70% higher than the estimate we would get by considering only the dominantly symmetric part of the wind stress (X_s). An analogous conclusion follows for $\hat{G}_{2n}$. Accordingly, we will consider the response to both symmetric and antisymmetric forcing, with the recognition that while the former is likely to be more important for the excitation of inertia–gravity waves in the Pacific, the latter should not be neglected.

(i) Idealized meridional structures of wind stress

As is clear from (41), a detailed analysis of the excitation of all modes requires full knowledge of the meridional structure of the wind stress in addition to its wavenumber–frequency dependence. In this work we will consider a few idealized meridional profiles, but they will provide an intuitive foundation for understanding the excitation by more general structures. The focus throughout is on the mode-by-mode wavenumber dependence.

Any particular mode can be forced by only one Hermite component of the meridional winds [see (40)]. The detailed meridional structure of the meridional wind thus affects the relative amplitudes of the various oceanic modes but is irrelevant to the wavenumber dependence of a single mode's response. We saw in section 2c that $U_{(m)}$ asymptotes toward $\psi_{m+1}(y)$ as $k \to \infty$ and toward $\psi_{m-1}(y)$ as $k \to -\infty$, with a mix of the two Hermite functions at small wavenumbers. There are thus two Hermite expansion coefficients of X that contribute to the excitation of a single mode, with one dominating at large positive wavenumbers and the other dominating at large negative wavenumbers. In the spirit of broadband forcing then, our first choice is a wind

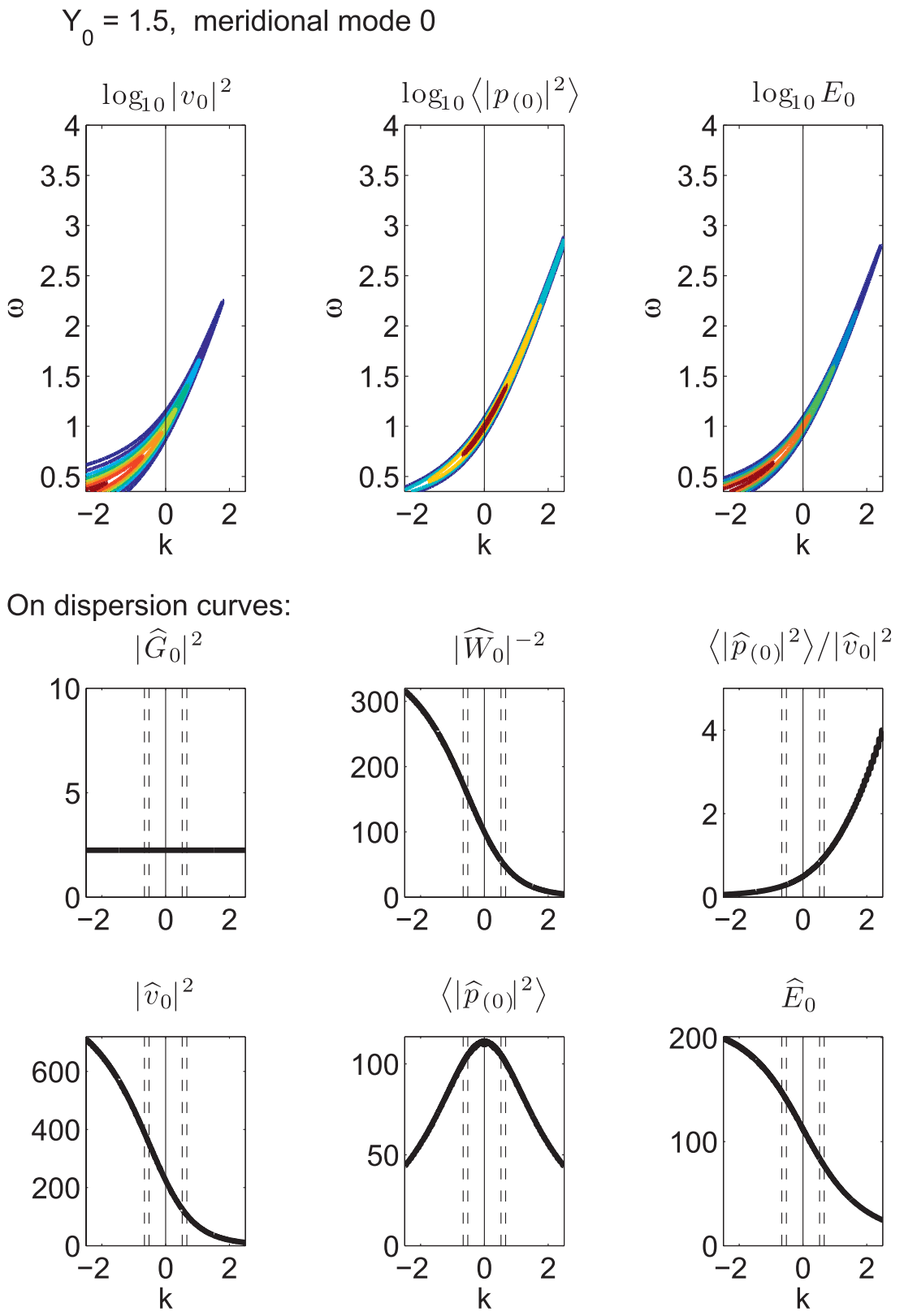

FIG. 9. Response of oceanic MRG wave to symmetric meridional winds with Hermite expansion coefficient $Y_0 = 1.5$. Figure format as in Fig. 5.

structure for which the Hermite expansion coefficients are all equal, so that the k-dependence of the $U_{(m)}$ structure has a minimal effect on the k-dependence of the resonance amplitude. This choice also distributes the meridionally integrated variance equally among the Hermite components of the wind stress, providing a qualitative complement to the broadband specification in zonal wavenumber and frequency. The top panel of Fig. 4 shows the resulting symmetric and antisymmetric structures.

The atmospheric length scales are typically larger than the oceanic ones (e.g., Wheeler and Kiladis 1999; Farrar and Durland 2012), and a reasonable lowest order approximation across the oceanic equatorial waveguide is to assume that the symmetric winds are uniform with latitude (an assumption used by WG) while the antisymmetric winds vary linearly with latitude. Accordingly, our second choice of idealized wind profiles is $X_s = 1$ and $X_a = y/2$, shown in the middle panel of Fig. 4. The effects of the symmetric and antisymmetric wind components will be considered separately, so the relative amplitudes of these choices do not matter; each is simply chosen to be $O(1)$.

Over the oceanic waveguide, the difference between the symmetric profiles in the top and middle panels of Fig. 4 is not great (true also for the difference between the two antisymmetric profiles). Nevertheless, we will see that the subtle differences will have a noticeable effect on the response to zonal winds because the Hermite expansion coefficients of the structures in the middle panel depend on the mode number. The lowest six of these coefficients are shown in the bottom panel of Fig. 4. For $X_s = 1$, the Hermite coefficients decrease with increasing mode number, so that compared to the constant X_m case, we expect the projection $\langle U_{(2n)} X_s \rangle$ to be relatively larger at negative wavenumbers where $U_{(2n)}$ is closer to ψ_{2n-1} than at positive wavenumbers where $U_{(2n)}$ is closer to ψ_{2n+1}. The situation is reversed for $X_a = y/2$. The expansion coefficients increase with increasing mode number, so we expect $\langle U_{(2n+1)} X_a \rangle$ to be relatively larger at positive than at negative wavenumbers.

(ii) Forcing by $Y_m = 1.5$

Figure 5 shows the solutions for forcing by purely meridional winds having the structures associated with constant Hermite expansion coefficients (Fig. 4, top panel). The symmetric oceanic modes (m odd) are excited by the antisymmetric $Y_a = 1.5\sum_{n=0}^{\infty}\psi_{2n+1}(y)$, and the antisymmetric oceanic modes (m even) are excited by the symmetric $Y_s = 1.5\sum_{n=0}^{\infty}\psi_{2n}(y)$. When the forcing consists only of broadband meridional winds, we can see in (41) that the forcing function will not depend on wavenumber because the structure and amplitude of $V_{(m)}$ do not. The choice of constant Hermite coefficients for the structure of the wind, combined with the ortho-normal property of the Hermite functions means that the forcing function also will be identical for all modes. This is seen in the middle row, left panel of Fig. 5, where the k-independent forcing functions of all four modes overlay each other. Because $V_{(m)}$ is equal to a single Hermite function, $\hat{G}_m$ will be k-independent under broadband forcing for any meridional structure of Y. A structure other than that used for Fig. 5 will only result in different amplitudes for different modes. The relative k dependence of any of the solutions in Fig. 5 for any particular mode would not be changed, so we do not need to consider other meridional structures for Y. Figure 5 tells us everything we need to know about the response of modes 1 to 4 individually to broadband meridional winds, symmetric or antisymmetric.

(iii) Forcing by $X_m = 1.5$

Figure 6 shows the response to purely zonal winds with the meridional structures shown in the top panel of Fig. 4. The symmetric oceanic modes (m odd) are excited by the symmetric $X_s = 1.5\sum_{n=0}^{\infty}\psi_{2n}(y)$, and the antisymmetric oceanic modes (m even) are excited by the antisymmetric $X_a = 1.5\sum_{n=0}^{\infty}\psi_{2n+1}(y)$. In contrast to the effects of meridional winds, the form of (41) together with our knowledge of the wavenumber dependence of $U_{(m)}$ makes it clear that under broadband zonal winds, the forcing function will be wavenumber dependent. The magnitude of $\hat{G}_m$ increases with increasing $|k|$, as the amplitude of $U_{(m)}$ does, and this is shown in the middle row, left panel of Fig. 6. There is a minimum in $|\hat{G}_m|^2$ near $k = 0$ that is most pronounced for the lowest meridional mode, and there is a skewing of the amplitude toward negative wavenumbers, which is also most pronounced for the lowest mode. This is because the amplitude of $U_{(m)}$ increases faster with increasing $|k|$ for negative wavenumbers because of the beta-skewing of the dispersion curves, as we saw in Section 2c.

(iv) Forcing by $X_s = 1$ and $X_a = y/2$

The response of symmetric modes 1 and 3 to uniform zonal forcing $X_s = 1$ is shown in Fig. 7, and the response of antisymmetric modes 2 and 4 to the antisymmetric forcing $X_a = y/2$ is shown in Fig. 8. As expected, the decrease in the Hermite coefficients with increasing mode number for $X_s = 1$ increases the skew in $|\hat{G}_m|^2$ toward negative wavenumbers, particularly for mode 1 (Fig. 7, middle row, left panel). The increasing Hermite coefficients of $X_a = y/2$ result in $|\hat{G}_m|^2$ structures for modes 2 and 4 that are slightly skewed toward positive

wavenumbers (Fig. 8, middle row, left panel). The important thing is that for all of the zonal forcing scenarios considered, there is a minimum in the forcing function near $k = 0$ because the waves asymptote toward pure gravity waves as $|k| \to \infty$, increasing the magnitude of the projection $\langle U_m X \rangle$.

2) DISPERSION FUNCTION AT RESONANCE

At resonance (i.e., on a dispersion curve), the dispersion function is

$$\hat{W}_m = i\epsilon\left(\frac{2\omega_m^2 + k/\omega_m}{\omega_m^2 - k^2}\right) + O(\epsilon^2). \tag{45}$$

The $O(\epsilon^2)$ term comes from the real part of $\hat{W}_m$, so the inverse squared magnitude is

$$|\hat{W}_m|^{-2} = \epsilon^{-2}\left(\frac{\omega_m^2 - k^2}{2\omega_m^2 + k/\omega_m}\right)^2 + O(1). \tag{46}$$

For inertia–gravity waves $|k/\omega_m| < 1$, so the denominator will clearly have a minimum near the minimum modal frequency ω_{cm}, producing a peak in $|\hat{W}_m|^{-2}$ near the locus of vanishing group velocity. The exact minimum of the denominator is shifted to a slightly more negative wavenumber by the k/ω_m term, but $(\omega_m^2 - k^2)^2$ [which varies only between $(2m)^2$ as $k \to -\infty$ and $(2m + 2)^2$ as $k \to \infty$, see (35)] acts oppositely. The peaks in $|\hat{W}_m|^{-2}$ are thus found at $k_{cm} < k < 0$ and the peak widths are skewed slightly toward positive wavenumbers. The asymmetries about $k = 0$ are subtle for mode 1 and decrease rapidly with increasing mode number. The dispersion function is of course independent of forcing, and the middle panel of the middle row in Fig. 5 shows the wavenumber dependence of $|\hat{W}_m|^{-2}$ for modes 1–4. These structures are repeated where appropriate in Figs. 6–8, but they are not different in those figures.

3) v AT RESONANCE

(i) Meridional forcing

The $|\hat{v}_m|^2$ solutions are simply the product of $|\hat{G}_m|^2$ and $|\hat{W}_m|^{-2}$ [see (23)]. For the case of meridional forcing, the wavenumber dependence of $|\hat{v}_m|^2$ is determined solely by the dispersion function, with a pronounced peak between $k = k_{cm}$ and $k = 0$, and a slight skewing of the peak width toward positive wavenumbers (left panel, bottom row, Fig. 5).

(ii) Zonal forcing

In the case of zonal forcing, the $|\hat{v}_m|^2$ peaks are attenuated somewhat by the minima in $|\hat{G}_m|^2$ near $k = 0$. When X_m is constant with mode number, the slight skewing of $|\hat{G}_m|^2$ toward negative wavenumbers acts in opposition to the slight skewing of $|\hat{W}_m|^{-2}$ toward positive wavenumbers, and $|\hat{v}_m|^2$ is nearly symmetric about its peak (left panel, bottom row, Fig. 6). When X is uniform in latitude, the strong skewing of $|\hat{G}_m|^2$ toward negative wavenumbers produces skewing of both the peak location and the peak width of $|\hat{v}_m|^2$ toward negative wavenumbers (left panel, bottom row, Fig. 7). For $X_a = y/2$, the peak in $|\hat{v}_m|^2$ falls very near $k = 0$, with a slight skewing of the the peak width toward positive wavenumbers. In all the cases we have examined, the meridional velocity variance ($|\hat{v}_m|^2$) does show a maximum that is at least near the locus of vanishing group velocity in wavenumber–frequency space. To see what this means in terms of SSH variability and the total wave energy, we now look at the conversion from $v_{(m)}$ to $p_{(m)}$ and $u_{(m)}$.

4) u AND p SOLUTIONS

On the free-wave dispersion curves, the forcing terms on the rhs of (5) and (6) are $O(\epsilon)$ relative to the resonant v terms. At resonance, then, we can disregard the forcing terms and derive expressions for $u_{(m)}$ and $p_{(m)}$ in terms of $v_{(m)}$ that are fully analogous to (10) and (11), with ω_m replaced by σ. For completeness sake, we will be a bit more careful and note that (5) and (6) seem to indicate that u and p are resonant on the asymptotes $\omega = \pm k$, even if v is not. Were we to proceed as above for the modal definitions over the larger wavenumber–frequency space, each individual meridional mode would show not only a resonance on the appropriate inertia–gravity wave dispersion curve, but also a $(u_{(m)}, p_{(m)})$ resonance on $\omega = \pm k$. This would show up in the wavenumber–frequency spectra of individual modes, for instance in the top rows of Figs. 5–8. There are two issues here. First, we must determine whether there truly are (u, p) resonances on $\omega = \pm k$, as hinted at by (5) and (6) and by the fact that these asymptotes satisfy the dispersion relations of the Kelvin wave and the two spurious solutions noted in Section 2b. Second, any resonance that does occur on $\omega = \pm k$ should be expressible as a separate entity rather than being lumped together with the resonance expressions of other modes.

In the appendix, we show that most of the apparent resonances on $\omega = \pm k$ are artifacts of our separation into individual meridional modes. In the case of zonal forcing, most of the X_m-related terms cancel with v_m-related terms on the asymptotes when the modes are summed. On $\omega = k$, the only term remaining represents the Kelvin wave resonance with the $X_0\psi_0$ forcing term. On $\omega = -k$, there is a resonance of u, v, and p only at $\omega = 1/\sqrt{2}$. This is the point at which the MRG wave

dispersion curve crosses $\omega = -k$, so this is really part of the MRG wave resonance. Under meridional forcing, v is $O(\epsilon)$ relative to the forcing on $\omega = \pm k$, so the apparent resonance in u and p only brings these terms up to $O(1)$ relative to the forcing (i.e., they are not resonant). Representations for $u_{(m)}$ and $p_{(m)}$ which are valid over the entire domain and which suppress the spurious resonances are given in (A17) and (A18). These equations were used to generate the relevant panels in Figs. 5–8.

5) $u_{(m)}$, $p_{(m)}$ AND E_m AT RESONANCE

At resonance, the forcing-related terms in (A17)–(A18) can be neglected because v_m is $O(\epsilon^{-1})$ there. With the restriction previously imposed that $\omega_m \pm k$ be $O(1)$, the relations between $(u_{(m)}, p_{(m)})$ and $v_{(m)}$ are then identical to the relations between the free wave components $(U_{(m)}, P_{(m)})$ and $V_{(m)}$ given in (10)–(11), with the modal amplitude v_m inserted as a multiplicative factor on the rhs of each equation. Neglecting higher order terms,

$$\langle|\hat{p}_{(m)}|^2\rangle/\langle|\hat{v}_{(m)}|^2\rangle = \langle|P_{(m)}|^2\rangle/\langle|V_{(m)}|^2\rangle \tag{47}$$

[see(17), (18), and Fig. 2],

$$\langle|\hat{p}_{(m)}|^2\rangle = |\hat{G}_m|^2|\hat{W}_m|^{-2}\langle|P_{(m)}|^2\rangle/\langle|V_{(m)}|^2\rangle, \tag{48}$$

$$\langle|\hat{u}_{(m)}|^2\rangle = \langle|\hat{p}_{(m)}|^2\rangle, \quad \text{and} \tag{49}$$

$$\hat{E}_m = |\hat{G}_m|^2|\hat{W}_m|^{-2}[1 + 2\langle|P_{(m)}|^2\rangle/\langle|V_{(m)}|^2\rangle]/4. \tag{50}$$

(i) Meridional forcing

The trough in $\langle|\hat{p}_{(m)}|^2\rangle/\langle|\hat{v}_{(m)}|^2\rangle$ at low wavenumbers (Fig. 5, middle row, right panel) almost balances the low-wavenumber peak in $\langle|\hat{W}_{(m)}|^{-2}\rangle$, so meridional forcing produces a very subtle maximum in $\langle|\hat{p}_{(m)}|^2\rangle$ at low wavenumbers (Fig. 5, bottom row, middle panel). The associated maximum in $\hat{E}_m$ is more pronounced. Over the wavenumber band resolvable by the TAO/TRITON array, $\langle|\hat{p}_{(m)}|^2\rangle$ is essentially flat, and the peak in $\hat{E}_m$ would probably not be detectable.

(ii) Zonal forcing

Under zonal forcing, the increase in both $\hat{G}_m$ and $\langle|\hat{p}_{(m)}|^2\rangle/\langle|\hat{v}_{(m)}|^2\rangle$ with increasing $|k|$ produces a minimum in $\langle|\hat{p}_{(m)}|^2\rangle$ at low wavenumbers for all scenarios. When X_m is constant there is a slight preference for the negative wavenumbers (middle panel, bottom row, Fig. 6). When X is uniform in y, the preference for excitation of $\langle|\hat{p}_{(m)}|^2\rangle$ at negative wavenumbers is pronounced in mode 1 and more subtle in mode 3 (Fig. 7, bottom row, middle panel). Under $X_a = y/2$ forcing, there is a slight preference for positive wavenumbers (Fig. 8, bottom row, middle panel).

The combination of the low wavenumber peak in $\langle|\hat{v}_{(m)}|^2\rangle$ and the low wavenumber trough in $\langle|\hat{p}_{(m)}|^2\rangle$ under zonal forcing produces an energy profile $[\hat{E}_m(k)]$ with neither peak nor trough at low wavenumbers in all scenarios (Figs. 6–8, bottom row, right panel). In the constant X_m scenario (Fig. 6), $\hat{E}_m$ is very nearly independent of both wavenumber and mode number. In the uniform X scenario (Fig. 7) there is a more noticeable preference for negative wavenumbers, particularly in mode 1, and for $X_a = y/2$ forcing (Fig. 8), $\hat{E}_m$ increases in the positive wavenumber direction.

The important points are that zonal forcing produces minima in $\langle|\hat{p}_{(m)}|^2\rangle$ at low wavenumbers, and near k-independence in $\hat{E}_m$ when the Hermite coefficients of X are constant. Other meridional structures of X produce predictable skews of these general structures toward negative wavenumbers when $X_{m+1} < X_{m-1}$ (e.g., $X_s = 1$) and toward positive wavenumbers when $X_{m+1} > X_{m-1}$ (e.g., $X_a = y/2$).

Near the limits of our wavenumber range, the zonal wavenumbers become as large as the meridional wavenumbers of the low modes, and we can no longer neglect the influence of zonal wavenumbers on the dissipation parameter. The increasing trend in $\hat{E}_m$ seen in the bottom-right panels of Figs. 7 and 8 would not continue as shown beyond the displayed wavenumber range. A more realistic parameterization of dissipation would increasingly attenuate the resonant energy as the zonal length scales become increasingly shorter.

6) FORCING EFFICIENCY AND THE INERTIA–GRAVITY WAVE TRANSFER FUNCTION

For descriptive purposes, we will use the term ''efficiency'' to reflect the response-to-forcing ratios seen in our mode-by-mode solutions. We have separated the resonant solutions into several parts, but we must remember that the separation was partially arbitrary, and the full transfer function from wind forcing to a particular oceanic resonance involves the product of these parts [e.g. (50)]. Under broadband meridional forcing, the part we have called the ''forcing function'' ($\hat{G}_m$) is wavenumber independent, while under broadband zonal forcing, $|\hat{G}_m|$ grows monotonically with increasing $|k|$. Because $\hat{G}_m$ is the only ''part'' of our solution that depends on the forcing, it is tempting to conclude that the efficiency of meridional forcing is independent of wavenumber, while the efficiency of zonal forcing increases with increasing $|k|$ as the waves asymptote toward pure

gravity waves. This is not the best interpretation, however, because the magnitude of the inverse dispersion function ($|\hat{W}_m|^{-1}$) decreases monotonically with increasing $|k|$, independently of the forcing, and this is as much a part of the resonant response as the forcing function.

Imposing constant Hermite expansion coefficients on the meridional structure of the wind is not quite the same as imposing wavenumber independence in Fourier space, but we have seen that it has a similar effect. Because $U_{(m)}$ asymptotes toward a ψ_{m-1} structure as $k \to -\infty$ and toward a ψ_{m+1} structure as $k \to \infty$, constant Hermite expansion coefficients for the zonal forcing X reduce the "bias" toward either positive or negative wavenumbers in the projection $\langle U_{(m)}X\rangle$. When $|\hat{G}_m|^2 = |\langle U_{(m)}X\rangle|^2$ is multiplied by the other components of the energy solution (50), each with its own slight asymmetry in k, the constant Hermite spectrum forces a total wave energy $\hat{E}_m$ that is nearly independent of wavenumber and meridional mode number (with a very slight increase toward negative wavenumbers: Fig. 6, bottom right panel).

We conclude that when the zonal winds are broadband in wavenumber and frequency, and the meridional structure of the wind has a "white" Hermite spectrum (X_m = a constant), the efficiency with which zonal winds excite total wave energy in meridional mode m is, to first approximation, independent of zonal wavenumber. Because $|\hat{G}_m|$ increases with increasing $|k|$ for zonal winds but remains constant for meridional winds, we conclude that under analogous conditions the efficiency with which meridional winds excite total wave energy in mode m decreases with increasing $|k|$. The difference in the wavenumber dependence of $\hat{E}_m$ between Figs. 5 and 6 is *only* due to the difference in the wavenumber dependence between $\langle V_{(m)}Y\rangle$ and $\langle U_{(m)}X\rangle$. The low-wavenumber peak in $\hat{E}_m$ under broadband meridional forcing (Fig. 5, bottom right panel) is therefore not the consequence of a vanishing group velocity, but is simply due to the decreasing importance of v in the wave structure with increasing $|k|$, which decreases the ability of the meridional winds to excite the waves.

The fact that wavenumber independence of the excitation efficiency is represented by a "forcing function" that increases with increasing $|k|$ is largely due to our convention for the "unit amplitude" free wave. Normalizing this wave by a wavenumber-dependent amplitude of $U_{(m)}$ rather than the amplitude of $V_{(m)}$ might have been more desirable physically, but the clarity of the results would likely have been lost in the added mathematical complexity.

We can consider the virtually constant $\hat{E}_m$ displayed in the bottom right panel of Fig. 6 to be a generic broadband transfer function from wind stress to oceanic mode m, from which we can deduce, at least qualitatively, the solutions for the other wind structures. Because of the known relation between $U_{(m)}$, $P_{(m)}$ and $V_{(m)}$, we know that the wavenumber independence of $\hat{E}_m$ implies a low-wavenumber peak in $|\hat{v}_m|^2$ and low-wavenumber troughs in $\langle|\hat{p}_{(m)}|^2\rangle$ and $\langle|\hat{u}_{(m)}|^2\rangle$, with the peak being more pronounced than the troughs. A meridional structure of X for which the Hermite expansion coefficients decrease with increasing mode number skews all of the above features toward negative wavenumbers, while a structure for which the expansion coefficients increase with increasing mode number skews the features toward positive wavenumbers. We have shown a few generic meridional structures for which the tendency of X_m is consistent from mode to mode, but for a particular meridional mode m, all that matters is the relative sizes of the two components X_{m+1} and X_{m-1}. When the forcing is due to broadband meridional winds, the skewing does not apply, but the decreasing forcing efficiency with increasing $|k|$ produces a low-wavenumber peak in $\hat{E}_m$, a correspondingly sharper low-wavenumber peak in $|\hat{v}_m|^2$, and barely noticeable low-wavenumber peaks in $\langle|\hat{p}_{(m)}|^2\rangle$ and $\langle|\hat{u}_{(m)}|^2\rangle$. The zonal-wavenumber and frequency content of nonbroadband winds can then be imposed directly on the above structures.

Our focus has been on the wavenumber structure of individual modes, but it should be remembered that any zonal wind in the proper wavenumber–frequency range excites more than one inertia–gravity mode because the $U_{(m)}$ are not mutually orthogonal. For example, a broadband wind with structure $X = \psi_2(y) + \psi_4(y)$ will excite inertia–gravity mode 3 with very little wavenumber dependence for total wave energy. It will also excite mode 1 with increasing efficiency as $k \to \infty$ and mode 5 with increasing efficiency as $k \to -\infty$. The tendencies of these latter two modes combine to reduce the wavenumber dependence of the total oceanic wave energy excited by X, but a more detailed analysis is beyond the scope of the present work.

c. *The forced MRG wave*

The $m = 0$ dispersion polynomial as defined in (8) vanishes along the spurious dispersion curve $\omega = -k$, but this root cancels with part of the $\omega^2 - k^2$ term in the denominator of the dispersion function W_0. The forms of the forcing function and dispersion function for the MRG wave are

$$G_0 = iY_0 + \frac{1}{\sqrt{2}(\sigma - k)}X_1, \quad \text{and} \tag{51}$$

$$W_0 = \sigma - \frac{1}{\sigma - k}. \tag{52}$$

Within our chosen wavenumber–frequency range $(\sigma - k) = (\omega - k)[1 + O(\epsilon)]$, so on the MRG wave dispersion curve, (51)–(52) reduce to

$$\hat{G}_0 = iY_0 + \frac{\omega}{\sqrt{2}} X_1[1 + O(\epsilon)]$$
$$= i[\langle V_{(0)} Y\rangle - \langle U_{(0)} X\rangle] + O(\epsilon), \quad \text{and} \qquad (53)$$

$$\hat{W}_0 = i\epsilon(1 + \omega^2) + O(\epsilon^2). \qquad (54)$$

As with the inertia–gravity waves, $V_{(0)} \equiv \psi_0(y)$ is independent of wavenumber in form and amplitude, so the part of the forcing function due to broadband meridional winds is independent of wavenumber. The latitudinal dependence of $U_{(0)}$ and $P_{(0)}$ does not depend on wavenumber, so X_1 is the only Hermite coefficient of X that contributes to the forcing function. Their amplitudes, however, increase monotonically with increasing frequency [see (19)–(20)], and hence wavenumber [see (12)]. Consequently, the zonal forcing function and $(\langle|\hat{p}_{(0)}|^2\rangle / \langle|\hat{v}_{(0)}|^2\rangle)$ increase monotonically with increasing wavenumber (rather than with increasing $|k|$), as the wave asymptotes toward a pure gravity wave.

1) MERIDIONAL FORCING

The inverse-squared magnitude of the dispersion function drops off rapidly with increasing frequency (and wavenumber), so $|\hat{v}_0|^2$ does also when the winds are meridional (Fig. 9, bottom row, left panel). The increase in $(\langle|\hat{p}_{(0)}|^2\rangle / \langle|\hat{v}_{(0)}|^2\rangle)$ with increasing wavenumber creates a strong pressure maximum near $k = 0$ in the presence of symmetric meridional winds (Fig. 9, bottom row, middle panel). It is worth noting that this enhancement of the resonant energy in the pressure signal occurs near vanishing wavenumber where the group velocity of the MRG wave is significant. It also bears little relation to the k-dependence of the total wave energy, which follows $|\hat{v}_0|^2$ and drops off rapidly and monotonically with increasing wavenumber (Fig. 9, bottom row, right panel).

2) ZONAL FORCING

Figure 10 shows the response to forcing by antisymmetric zonal winds, where the amplitude of X_1 was chosen equal to that of Y_0 in Fig. 9. The increase in $\hat{G}_0$ with increasing wavenumber creates a maximum in $|\hat{v}_0|^2$ at $k = 0$, and results in both $\langle|\hat{p}_{(0)}|^2\rangle$ and $\hat{E}_0$ increasing monotonically with increasing wavenumber (Fig. 10, bottom row).

A comparison of the bottom–middle panels of Figs. 9 and 10 shows that $X_1 = 1.5$ and $Y_0 = 1.5$ excite roughly the same magnitude of pressure variance near the positive Nyquist wavenumber of the TAO/TRITON array. At $k = 0$, $X_1 = 1.5$ excites roughly half the pressure variance of $Y_0 = 1.5$, and at the negative Nyquist wavenumber this ratio drops to roughly one quarter because of the decreasing relative importance of $U_{(1)}$ to the MRG wave structure as $k \to -\infty$.

4. Summary

We have had two main goals in this article, the first being to demonstrate that in the presence of broadband forcing of the equatorial oceans, the wavenumber–frequency loci of vanishing group velocity (k_{cm}, ω_{cm}) are not places where we should necessarily expect elevated inertia–gravity wave energy, particularly not in pressure-related measurements such as sea level or dynamic height. The order-of-magnitude analysis of WG does not predict more resonant energy at (k_{cm}, ω_{cm}) than at any other wavenumber along a dispersion curve, in spite of occasional claims to the contrary. The $O(\epsilon^{-1/2})$ enhancement that WG predicted at ω_{cm} relative to higher frequencies in a frequency spectrum results from the larger wavenumber band that contributes at ω_{cm} to the k-integral of the wavenumber–frequency spectrum.

Going beyond order-of-magnitude solutions, the efficiency with which broadband zonal winds excite total wave energy in a particular inertia–gravity mode is virtually wavenumber independent when the meridional structure of the wind has a "white" Hermite spectrum (X_m = a constant). The nearly constant $\hat{E}_m(k)$ is associated with a peak in meridional velocity variance and a trough in pressure variance at low wavenumbers, simply because v becomes progressively less important to the wave structure with increasing $|k|$. When the meridional structure of the zonal winds is such that the Hermite expansion coefficients (X_m) decrease with increasing mode number (as with meridionally uniform winds), the above structures are skewed toward negative wavenumbers. When X_m increases with increasing mode number (as with winds that depend linearly on latitude), the structures are skewed toward positive wavenumbers.

By contrast, the efficiency with which meridional winds excite total wave energy in the inertia–gravity modes falls off rapidly with increasing $|k|$, as v becomes a progressively less important component of the waves. Total-wave-energy peaks at low wavenumbers under meridional forcing are the consequence of this effect rather than of vanishing group velocity. Relative to the zonal forcing response, the low-wavenumber peak in meridional velocity variance is enhanced under meridional forcing. The pressure variance exhibits a weak maximum at low wavenumbers under meridional forcing, but within the wavenumber band resolvable by the TAO/TRITON array, it is virtually wavenumber independent.

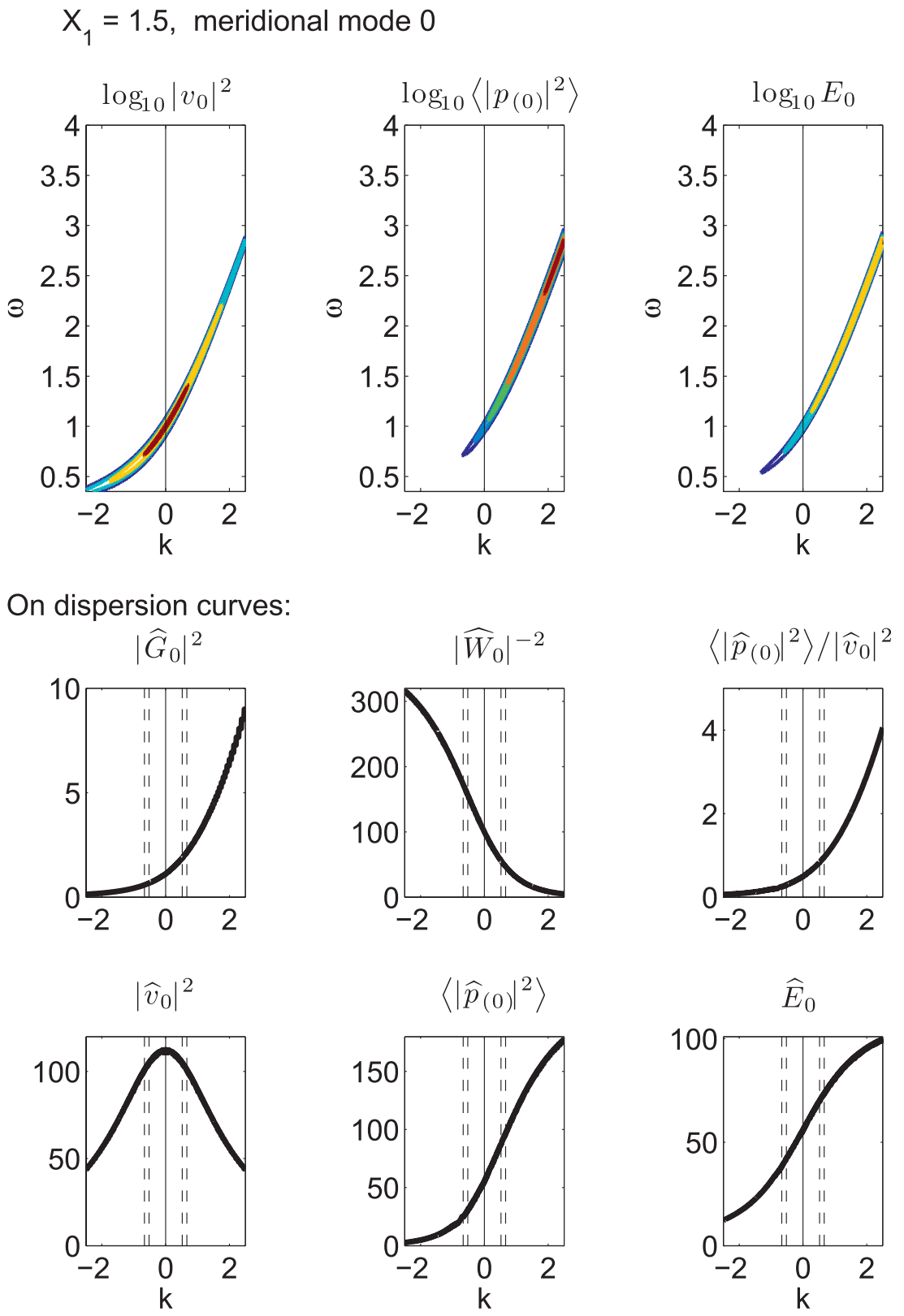

FIG. 10. Response of oceanic MRG wave to antisymmetric zonal winds with Hermite expansion coefficient $X_1 = 1.5$. Figure format as in Fig. 5.

Although their analysis did not address an isolated forcing region, WG did suggest that in such a region it is physically reasonable to expect a vanishing group velocity to produce an enhancement of resonant energy. Energy can escape the forcing region when the group velocity does not vanish but accumulates when the group velocity does vanish. We agree with this point under the proper conditions and with certain caveats. Locally, the resonant energy will be a balance of the energy input by the forcing, the energy dissipation (proportional to the wave energy) and the energy flux divergence of the wave field itself. When the group velocity vanishes, this latter term does also, and the resonance can grow to its full potential. When the group velocity does not vanish, the energy flux divergence can reduce the resonance amplitude, but this term depends as much on the gradient of the energy density as it does on the group velocity. In the case of a single sinusoid of uniform amplitude, the energy flux is equal to the period-averaged energy density times the formal group velocity (e.g., MP), but there is no gradient of the period-averaged energy density. The energy flux divergence thus vanishes regardless of the value of the group velocity. An isolated forcing patch will produce a spectrum of wavenumbers with fixed phase relations and in general, a nonzero energy density gradient. We can, however, imagine a case where the gradient is small enough that locally the energy flux divergence for a given group velocity remains small compared to the dissipation, and local reduction of the resonant energy is therefore minimal. Basin-scale forcing of the Pacific, with maximum amplitude in midbasin and diminishing amplitude toward the boundaries, might provide such a scenario.

A simple application of Parseval's Theorem shows that globally there is no reduction of resonant energy even in the case of isolated forcing, unless we account for special energy sinks not included in our model. The problem as we have formulated it is linear, and the wavenumber–frequency spectrum of the response depends only on the magnitudes of the wavenumber–frequency components of the forcing. In the case of localized forcing there are specific phase relations between the wavenumber components, but the wavenumber–frequency spectrum and hence the domain-integrated energy remains the same as if the phases were randomized and the solution consisted of uncorrelated pure sinusoids, each with no energy flux divergence. Physically, this just means that, if the resonant energy is reduced locally in an isolated forcing region because of a nonvanishing group velocity, the lost energy will still be found within the domain, but ''downstream'' of the forcing region.

The group velocity becomes important, of course, when it can transport energy to special regions of enhanced dissipation or modal scattering, such as lateral boundaries or changes in bathymetry. Luther (1980, p. 175), noted the likelihood of baroclinic-mode scattering as waves propagate out of the deep, relatively flat abyssal basin of the central Pacific, and of meridional-mode scattering when the waves reflect from the eastern and western boundaries (e.g., Moore 1968; MP). Both of these mechanisms could drain energy from the wind-forced modes, and the importance of such mechanisms merits further study. As previously mentioned, however, a very gradual decline in wind stress and resonant energy toward the boundaries could mitigate the impacts of such sinks by reducing the energy flux divergence in the presence of nonvanishing group velocity while simultaneously reducing the energy flux into the scattering regions. Farrar and Durland (2012) for instance, show some spectral peaks in oceanic energy at wavenumbers near k_{cm}, and other equally energetic peaks at wavenumbers distinctly removed from k_{cm}. It is not possible to determine from their analysis whether these latter peaks might have been partially attenuated by the nonvanishing group velocity, and this possibility also merits further study.

Finally, we emphasize that although the specific locus of vanishing group velocity may not be particularly special in the wavenumber–frequency domain, the modal frequency minimum associated with vanishing group velocity does have special significance for physical space, for the simple reason that a wider band of wavenumbers is available for resonant excitation at this frequency than at any other. When the forcing is narrow-banded in wavenumber this special significance is diminished or lost.

The datasets now available from satellite altimetry and scatterometry open up new opportunities to pursue the investigations suggested above and to develop a more complete understanding of how the equatorial ocean is responding to winds in the 3–20-day period range. The second major purpose of this paper, then, has been to review and refine the mathematical framework within which such analyses can be carried out, while establishing the baseline wavenumber–frequency dependence of the oceanic response to generic forcing, as predicted by linear theory.

Acknowledgments. We thank Carl Wunsch, Jay McCreary, Ken Brink, and Roger Samelson for enlightening discussions. We also thank Dennis Moore, Carl Wunsch, and Billy Kessler for reviews that significantly improved the paper. This research was funded by NASA Grant NNX10AO93G and is a contribution of the Ocean Vector Winds Science Team.

APPENDIX

Suppression of Spurious Resonance

a. Raising and lowering operators for Hermite functions

$$(y - d/dy)\psi_m = \sqrt{2(m+1)}\psi_{m+1}, \quad m = 0, 1, 2, \ldots, \tag{A1}$$

$$(y + d/dy)\psi_m = \begin{cases} 0, & m = 0, \\ \sqrt{2m}\psi_{m-1}, & m = 1, 2, 3, \ldots, \end{cases} \text{ and} \tag{A2}$$

$$(y^2 - d^2/dy^2)\psi_m = (2m+1)\psi_m. \tag{A3}$$

b. Real and spurious resonances in u and p on $\omega = \pm k$

Equations (5) and (6) make it appear that resonances in u and p can occur on $\omega = \pm k$, particularly in the presence of zonal forcing. If expressions for $u_{(m)}$ and $p_{(m)}$ are derived from our expression for $v_{(m)}$ by ignoring the X terms in (5)–(6), such resonances do in fact show up in the wavenumber–frequency spectra of each mode m. We show here that most of these resonances vanish in the sum of all modes. They are thus artifacts of our modal separation that can be removed by properly distributing the forcing components among the expressions for the individual meridional modes.

In what follows, we will retain the lowest-order term associated with X and also that associated with Y even if these two terms are different orders of ϵ, so that we can envision the effects of meridional and zonal forcing independently. Only terms that are $O(\epsilon^{-1})$ relative to the forcing are resonant. Terms that are $O(1)$ or smaller are part of the background (the nonresonant forced response).

Using the Hermite expansion of v, (5) and (6) can be expressed as

$$\begin{pmatrix} u \\ p \end{pmatrix} = \frac{i}{\sigma^2 - k^2}\left\{ \begin{pmatrix} \sigma \\ k \end{pmatrix} X + \sum_{m=0}^{\infty} v_m \left[(\sigma + k)\sqrt{\frac{m+1}{2}}\psi_{m+1} \pm (\sigma - k)\sqrt{\frac{m}{2}}\psi_{m-1} \right] \right\}, \tag{A4}$$

where the upper and lower signs in $\pm$ apply to u and p respectively, and $\psi_{-1} \equiv 0$.

On $\omega = k$, (24), (25) and (A4) are

$$G_m = i\left\{ Y_m - \epsilon^{-1}\left[\sqrt{\frac{m+1}{2}} X_{m+1} + O(\epsilon) \right] \right\}, \tag{A5}$$

$$W_m = i\epsilon^{-1}(m+1) + O(1), \quad \text{and} \tag{A6}$$

$$p = u = (2\epsilon)^{-1}\left[X + \sum_{m=0}^{\infty} \frac{G_m}{W_m}\sqrt{2(m+1)}\psi_{m+1} + O(\epsilon) \right]. \tag{A7}$$

Incorporating (A5) and (A6), (A7) becomes

$$p = u = \sum_{m=0}^{\infty} \frac{Y_m}{\sqrt{2(m+1)}}\psi_{m+1} + (2\epsilon)^{-1}\left(X - \sum_{m=0}^{\infty} X_{m+1}\psi_{m+1} \right) \tag{A8}$$

$$= \sum_{m=0}^{\infty} \frac{Y_m}{\sqrt{2(m+1)}}\psi_{m+1} + (2\epsilon)^{-1} X_0 \psi_0. \tag{A9}$$

The term containing Y_m is $O(1)$ and is therefore not resonant. Only the $X_0\psi_0$ component of X produces a resonance on $\omega = k$: the resonant Kelvin wave.

On $\omega = -k$ we have

$$G_m = \begin{cases} i\left[Y_m - \epsilon^{-1}\left(\sqrt{\frac{m}{2}} X_{m-1} + O(\epsilon) \right) \right], & m \geq 1 \\ iY_0 + \frac{1}{2\sqrt{2}\omega} X_1 + O(\epsilon), & m = 0 \end{cases} \tag{A10}$$

$$W_m = \begin{cases} i\epsilon^{-1} m + O(1), & m \geq 1 \\ (\omega - 1/2\omega) + i\epsilon(1 + 1/4\omega^2) + O(\epsilon^2), & m = 0 \end{cases} \tag{A11}$$

$$\begin{pmatrix} u \\ p \end{pmatrix} = (2\epsilon)^{-1}\left[\pm X \pm \sum_{m=1}^{\infty} \frac{G_m}{W_m}\sqrt{2m}\psi_{m-1} + i\epsilon \frac{G_0}{\sqrt{2}W_0}\psi_1 + O(\epsilon) \right]. \tag{A12}$$

We have retained the $\epsilon G_0/W_0$ term in (A12) because we will see that it can become dominant at $\omega = 1/\sqrt{2}$. Substituting (A10) and (A11) into (A12) produces

$$\begin{pmatrix} u \\ p \end{pmatrix} = \pm \sum_{m=1}^{\infty} \frac{Y_m}{\sqrt{2m}}\psi_{m-1} \pm (2\epsilon)^{-1}\left(X - \sum_{m=1}^{\infty} X_{m-1}\psi_{m-1} \right) + \frac{i}{2\sqrt{2}} \frac{G_0}{W_0}\psi_1 \tag{A13}$$

$$= \pm \sum_{m=1}^{\infty} \frac{Y_m}{\sqrt{2m}}\psi_{m-1} + \frac{i}{2\sqrt{2}} \frac{G_0}{W_0}\psi_1. \tag{A14}$$

The first term on the rhs of (A14) is $O(1)$, and we can see from (A10) and (A11) that the second term is

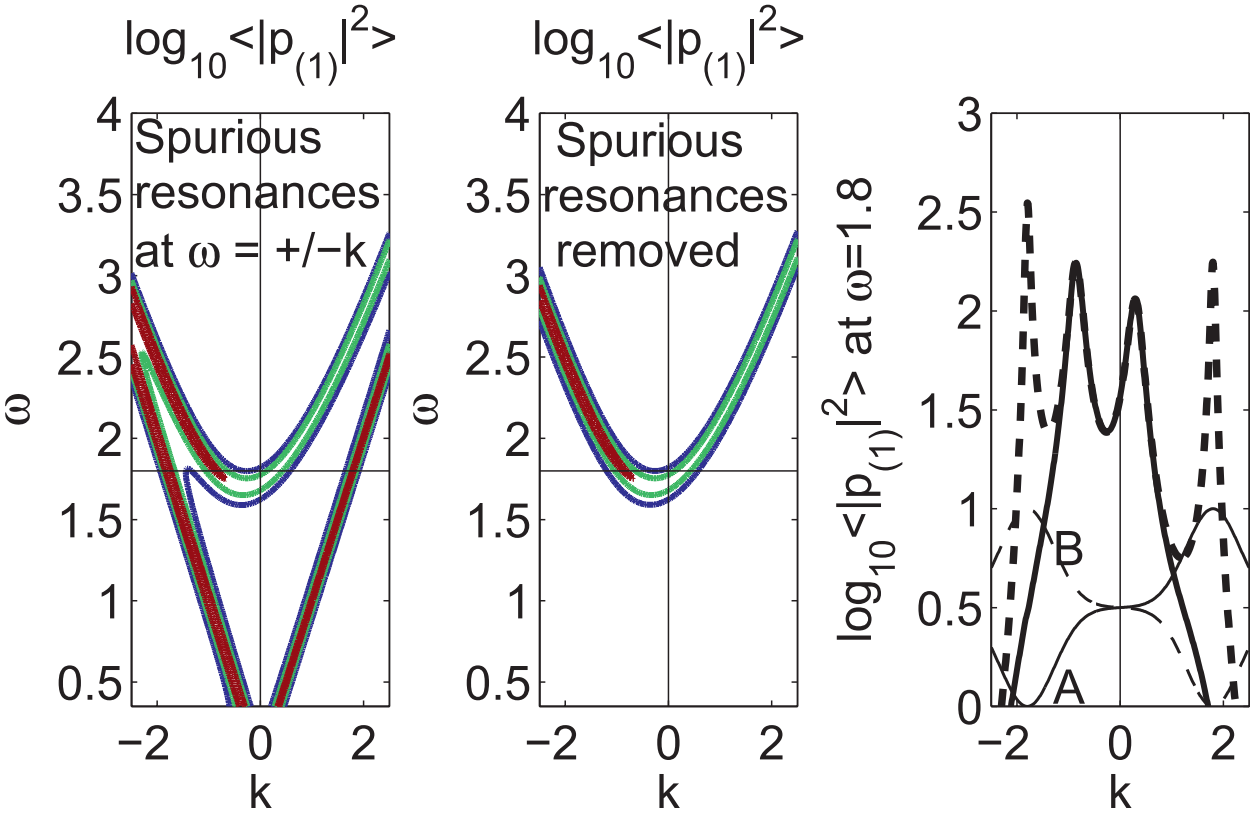

FIG. A1. Suppression of spurious resonances. Wavenumber–frequency spectra for inertia–gravity mode 1 forced by $X = 1$ when the forcing terms in (A18) are (left) not included and (middle) included. (right) Transect through the previous two panels at $\omega = 1.8$ (horizontal lines in left two panels). Displayed is $\langle |p_{(1)}|^2 \rangle$ vs k when the forcing terms in (A18) are (solid) included and (dashed) not included. Also shown are the wavenumber dependencies of (solid) $A(k, \omega)$ and (dashed) $B(k, \omega)$ at $\omega = 1.8$.

also $O(1)$ when $2\omega^2 - 1 = O(1)$. When $2\omega^2 - 1 = 0$, however,

$$v_0 = G_0/W_0 = \epsilon^{-1}(2Y_0 - iX_1)/3 \tag{A15}$$

and $$p = u = iv_0\psi_1/(2\sqrt{2}). \tag{A16}$$

Hence, u, p and v are resonant on $\omega = -k$ only at $\omega = 1/\sqrt{2}$. This is the frequency at which the MRG wave dispersion curve intersects $\omega = -k$, and indeed (A15) and (A16) exhibit the MRG wave structure. We have not found a resonance unique to $\omega = -k$ but merely have located one point on the MRG wave resonance curve. In short, the only resonance peculiar to $\omega = \pm k$ is the Kelvin wave resonance, which is excited by the $X_0\psi_0$ component of X on $\omega = k$, and in which u and p (but not v) are resonant.

Using the insights revealed above, definitions for the forced modal structures of u and p that do not exhibit spurious resonances on $\omega = \pm k$ are

$$\begin{aligned} u_{(m)}(y) &= i\left[\sqrt{\frac{m+1}{2}}\frac{v_m}{\sigma - k} + \frac{\sigma}{\sigma^2 - k^2}A(k,\omega)X_{m+1}\right]\psi_{m+1}(y) \\ &\quad + i\left[\sqrt{\frac{m}{2}}\frac{v_m}{\sigma + k} + \frac{\sigma}{\sigma^2 - k^2}B(k,\omega)X_{m-1}\right]\psi_{m-1}(y), \end{aligned} \tag{A17}$$

$$\begin{aligned} p_{(m)}(y) &= i\left[\sqrt{\frac{m+1}{2}}\frac{v_m}{\sigma - k} + \frac{k}{\sigma^2 - k^2}A(k,\omega)X_{m+1}\right]\psi_{m+1}(y) \\ &\quad - i\left[\sqrt{\frac{m}{2}}\frac{v_m}{\sigma + k} - \frac{k}{\sigma^2 - k^2}B(k,\omega)X_{m-1}\right]\psi_{m-1}(y). \end{aligned} \tag{A18}$$

In (A17) and (A18),

$$(A, B) = \begin{cases} (0,1) & \text{on} \quad \omega = -k \\ (1,0) & \text{on} \quad \omega = k, \end{cases} \tag{A19}$$

$$A \geq 0 \quad \text{and} \quad B \geq 0 \quad \text{for all } (k,\omega), \tag{A20}$$

$$\text{and} \quad A + B = 1 \quad \text{for all } (k,\omega). \tag{A21}$$

Using the definitions (A17)–(A21), Eqs. (5) and (6) can be rewritten in terms of the discrete forced modes:

$$u(y) = \frac{i\sigma}{\sigma^2 - k^2} A X_0 \psi_0(y) + \sum_{m=0}^{\infty} u_{(m)}(y), \tag{A22}$$

$$p(y) = \frac{ik}{\sigma^2 - k^2} A X_0 \psi_0(y) + \sum_{m=0}^{\infty} p_{(m)}(y). \tag{A23}$$

The resonant Kelvin wave is now obvious as a separate expression, and $u_{(m)}$ and $p_{(m)}$ are resonant only on the free-wave dispersion curve of mode $m \geq 0$. There is no resonance on $\omega = -k$ aside from the MRG wave resonance where the MRG wave dispersion curve crosses this line at $(k,\omega) = (-1/\sqrt{2}, 1/\sqrt{2})$.

The specifications (A19)–(A21) do not define A and B uniquely, but there is little value in seeking precise definitions if our focus is on the resonant solutions. $A(k,\omega)$ must vanish at $\omega = -k$, with an associated valley that is at least as wide as the spurious resonance peak at $\omega = -k$. The same is true of $B(k,\omega)$ in the neighborhood of $\omega = k$. Other than that, A and B act on terms that are $O(\epsilon)$ relative to the resonances and we are not concerned with their precise values. For the sole purpose of avoiding spurious $\omega = \pm k$ resonances in the formal definitions of the individual modes, a simple choice is sufficient:

$$\mathrm{A} = [1 + \exp\{-6(1 - k/\omega)^2\} - \exp\{-6(1 + k/\omega)^2\}]/2, \tag{A24}$$

$$B = [1 - \exp\{-6(1 - k/\omega)^2\} + \exp\{-6(1 + k/\omega)^2\}]/2. \tag{A25}$$

The difference between including and not including the forcing terms in (A18) can be seen in Fig. A1, where we show wavenumber–frequency spectra for the pressure signal of mode 1 when the terms are not included (left panel) and included (center panel). The right panel shows a transect through the left two panels at $\omega = 1.8$, together with the wavenumber dependence of A and B at that frequency.

REFERENCES

Blandford, R., 1966: Mixed gravity–Rossby waves in the ocean. *Deep-Sea Res.,* **13,** 941–961.

Farrar, J. T., and T. S. Durland, 2012: Wavenumber–frequency spectra of inertia–gravity and mixed Rossby–gravity waves in the equatorial Pacific Ocean. *J. Phys. Oceanogr.,* **42,** 1859–1881.

Ferrari, R., and C. Wunsch, 2010: The distribution of eddy kinetic and potential energies in the global ocean. *Tellus,* **62A,** 92–108.

Garzoli, S., and E. J. Katz, 1981: Observations of inertia–gravity waves in the Atlantic from inverted echo sounders during FGGE. *J. Phys. Oceanogr.,* **11,** 1463–1473.

LeBlond, P. H., and L. A. Mysak, 1978: *Waves in the Ocean.* Elsevier Science Publishers, 602 pp.

Lin, X., J. Yang, D. Wu, and P. Zhai, 2008: Explaining the global distribution of peak-spectrum variability of sea surface height. *Geophys. Res. Lett.,* **35,** L14602, doi:10.1029/2008GL034312.

Longuet-Higgins, M. S., 1965: Planetary waves on a rotating sphere II. *Proc. Roy. Soc. London,* **A284,** 40–68.

Luther, D. S., 1980: Observations of long period waves in the tropical oceans and atmosphere. Ph.D. thesis, MIT-WHOI Joint Program in Oceanography, Cambridge and Woods Hole, 210 pp.

Matsuno, T., 1966: Quasi-geostrophic motions in the equatorial area. *J. Meteor. Soc. Japan,* **44,** 25–42.

McPhaden, M. J., and R. A. Knox, 1979: Equatorial Kelvin and inertio-gravity waves in zonal shear flow. *J. Phys. Oceanogr.,* **9,** 263–277.

Moore, D. W., 1968: Planetary–gravity waves in an equatorial ocean. Ph.D. thesis, Harvard University, 200 pp.

——, and S. G. H. Philander, 1977: Modeling of the tropical ocean circulation. *The Sea,* E. D. Goldberg, Ed., *Marine Modeling,* Vol. 6, John Wiley and Sons, 319–361.

Pedlosky, J., 2003: *Waves in the Ocean and Atmosphere.* Springer-Verlag, 260 pp.

Wheeler, M., and G. N. Kiladis, 1999: Convectively coupled equatorial waves: Analysis of clouds and temperature in the wavenumber–frequency domain. *J. Atmos. Sci.,* **56,** 374–399.

Wunsch, C., and A. E. Gill, 1976: Observations of equatorially trapped waves in Pacific sea level variations. *Deep-Sea Res.,* **23,** 371–390.